Filamentary Magnetic Fields In Radio Galaxy Hotspots

A Thesis

submitted to

Indian Institute of Science Education and Research Pune

in partial fulfillment of the requirements for the

BS-MS Dual Degree Programme

by

Nishant Raina

Indian Institute of Science Education and Research Pune

Dr. Homi Bhabha Road,

Pashan, Pune 411008, INDIA.

May, 2019

Supervisor: Prasad Subramanian

Certificate

This is to certify that this dissertation entitled Filamentary Magnetic Fields In Radio Galaxy Hotspots towards the partial fulfilment of the BS-MS dual degree programme at the Indian Institute of Science Education and Research, Pune represents study/work carried out by Nishant Raina at Indian Institute of Science Education and Research under the supervision of Prasad Subramanian, Associate Professor, Department of Physics, during the academic year 2018-2019.

Prasad Subramanian

Committee:
Prasad Subramanian
Arijit Bhattacharyay

This thesis is dedicated to my late grandfather and friend, Sh. Makhan Lal Raina, who wished that I would one day become a doctor.

Declaration

I hereby declare that the matter embodied in the report entitled Filamentary Magnetic Fields In Radio Galaxy Hotspots are the results of the work carried out by me at the Department of Physics, Indian Institute of Science Education and Research, Pune, under the supervision of Prasad Subramanian and the same has not been submitted elsewhere for any other degree.

Nishant Raina

Acknowledgements

x

Abstract

The **standard model of synchrotron spectra** was developed by Westfold (1959), Ginzburg and Syrovatskii (1969) and also Pacholczyk (1970). Unlike the non-relativistic case, where the particle radiates at a single frequency, a relativistic particle emits at a range of frequencies. One of the main results of the papers by Westfold and the others is that the total power/emissivity radiated per unit frequency (assuming a power law distribution function for particle energies) is a decaying power law in frequency for all frequencies. However, such a nice form arises only under the set of assumptions that the magnetic field is uniform everywhere and that there is no upper limit on particle energies. In our work, we have been examining the consequences of filamentary magnetic field structures and their possible signatures on the observed spectrum at radio frequencies.

Contents

List of Figures

List of Tables

Chapter 1

Introduction

Astrophysical jets are awe eliciting cosmological phenomenon studied by theoretical astro-physicists and experimentalists alike. The scales at which these jets operate are truly remarkable in both size and extent. Technically speaking, astrophysical jets are highly collimated elongated beams of ionized matter emitted along the axis of rotation of exotic astronomical sources like radio galaxies, pulsars, quasars and black holes. The strong magnetic field produced by these dense nuclear objects forces these jets to be highly collimated. If the velocity of matter/plasma in such jets approaches the speed of light, we call them relativistic jets as they start showing effects from the theory of special relativity. Capable of extending to mega parsecs, such jets can excite surrounding sheaths of stationary gas or continuously supply an active region at the point where they terminate. These impact regions are called hotspots in extra-galactic terminology and are part of larger structures called radio lobes. Figure (1) shows a Fanaroff and Riley (FRII) Double Radio source.
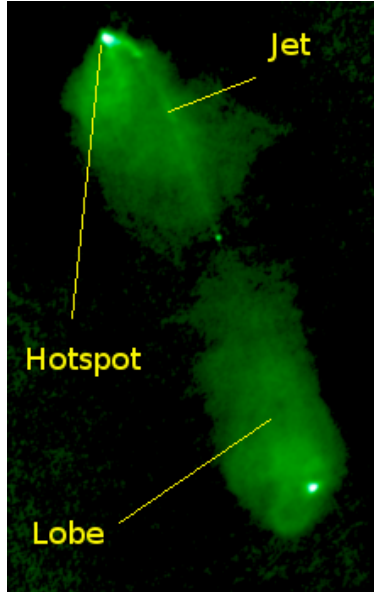
Figure 1.1: A classic FRII (double). Source: https://en.wikipedia.org

The characteristic temperature (or more accurately, the spectral dependence of the brightness versus wavelength) of a hot spot can be used to reveal the nature of the physical processes at work. The physical processes responsible for the radiation (at frequencies ranging from radio to X-rays) in such hotspots have been a subject of research since the eighties. However, answers to some important questions are still inconclusive - for instance, are the electrons responsible for the radiation re-accelerated in the vicinity of the hotspot or not, for the detection of such synchrotron electrons that are observed at such huge distances from the central source would otherwise be impossible as their energy (or equivalently, the Lorentz factor γ) would decay over time and they would run out of 'fuel' before they even reach the distances at which they are observed.

The physical mechanism that gives rise to the radiation from such hotspots/lobes is now widely believed to be synchrotron radiation. A synchrotron is a relativistic cyclotron but with several important differences arising out of relativistic effects which make it an interesting and intellectually stimulating problem in itself. An important difference is that unlike the non-relativistic case, where the particle radiates at a single frequency, a relativistic particle emits at a range of frequencies. We shall briefly derive the basics of synchrotron radiation in the subsequent sections but the reader may read up any textbook that deals with radiation fields for relevant concepts. In particular, one may want to start with:

- Radiative Processes In Astrophysics by G.B. Rybicki, and A.P. Lightman, 2004 Wiley-

VCH Edition. It uses the Guassian-CGS unit system.

- High Energy Astrophysics by Malcolm S. Longair, 2011 Cambridge University Press, 3rd Edition. This one uses the SI system of units.

Chapter 2

Theoretical Foundations

2.1 Larmor's Formula

Larmor's formula arises when one tries to find out the radiation emitted from an accelerated charge. Although it is possible to derive this formula directly from Maxwell's Equations, we shall instead be using the much simpler and intuitive approach that was taken by J.J Thomson. The latter helps give a better physical understanding of the phenomenon and is mathematically far less intricate than the actual derivation. This derivation shall make use of the Gaussian-CGS system of units.

For a stationary point charge, **Coulomb's Law** dictates that the the electric field E be purely in the radial direction:

$$E = E_r = \frac{q}{r^2}$$

Let us say that the charged particle is accelerated by a small velocity $\triangle v$ in some time $\triangle t$. After a time t, the pure radial electric fields lines shall be disrupted and there will be a perpendicular component of the electric field as well:

$$\frac{E_\perp}{E_r} = \frac{\triangle vtsin\theta}{c\triangle t} \tag{2.1}$$

Figure 2.1 (taken from Longair, Pg-156) helps explain how the above expression can be obtained:
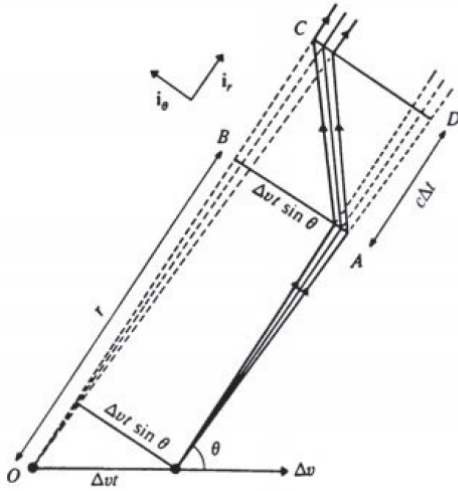
Figure 2.1: Perpendicular and Radial Electric fields. (Source: Rybicki and Lightman)

Substituting $t = r/c$ in the 2.1 gives the perpendicular component of the electric field:

$$E_\perp = \frac{q}{r^2}\left(\frac{\triangle v}{\triangle t}\right)\frac{r sin\theta}{c^2} = \frac{q\dot{v}sin\theta}{rc^2} \tag{2.2}$$

An important point to note here is that $E_\perp$ depends on r^{-1} and not r^{-2} like the radial field. Thus far away from the charge, only $E_\perp$ will contribute significantly to the radiation field.

Next comes the question of total power radiated in each direction. This requires us to make use of the *Poynting Vector S*. In CGS units, S is proportional to the square of the perpendicular component of the electric field:

$$|\boldsymbol{S}| = \frac{c}{4\pi}E_\perp^2 \tag{2.3}$$

Putting in the value of $E_\perp$ from Equation 2.2, we obtain the famous **Larmor's formula**.

$$|\boldsymbol{S}| = \frac{1}{4\pi}\left(\frac{q^2\dot{v}^2sin^2\theta}{c^3r^2}\right) \tag{2.4}$$

The charge radiates with a dipolar power pattern that looks like a doughnut whose axis is parallel to $\dot{v}$. Figure 2.2 (taken from www.cv.nrao.edu) shows the angular distribution of the radiation diagrammatically.
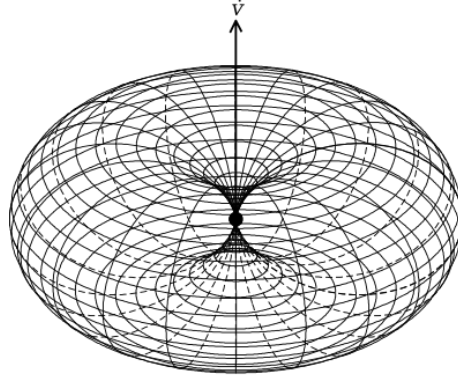
Figure 2.2: Doughnut shaped angular distribution of radiation. (Source: https://www.cv.nrao.edu)

In order to find the total power radiated in all directions, one must integrate 2.4 over all directions. Although trivial, we shall not show the entire calculation here. The total emitted power comes out to be:

$$P = \int |\boldsymbol{S}| \, dA = \frac{2}{3}\frac{q^2\dot{v}^2}{c^3} \tag{2.5}$$

This result is known as the **Larmor's Equation**. According to 2.5, the total (integrated) power radiated over all the directions is proportional to the square of the acceleration of the charged particle.

The relativistic generalization of the Larmor's formula uses relativistic transformations to and from the particle's instantaneous rest frame. The same can be found in any standard textbook for e.g. Rybicki and Lightman. The important result to be noted, however, is that the total power P is in some sense, the sum of the squares of the perpendicular and parallel components of acceleration of the charged particle.

$$P = \frac{2q^2}{3c^3}\gamma^4 \left(a_\perp^2 + \gamma^2 a_\parallel^2\right) \tag{2.6}$$

2.2 Relativistic Beaming

One can find the derivations of the general expressions for the angular distribution of received power in either Rybicki & Lightman or Longair's book. It suffices to say that the derivations require the Lorentz transformations of the angular distributions of emitted power. For purposes relevant to us, we shall only look at the expressions where the acceleration of the

point charge is either parallel or perpendicular to the direction of the velocity and then arrive at relativistic limits for such cases. To make these expressions easier to understand, we believe is necessary to include the following figure taken from Rybicki & Lightman:
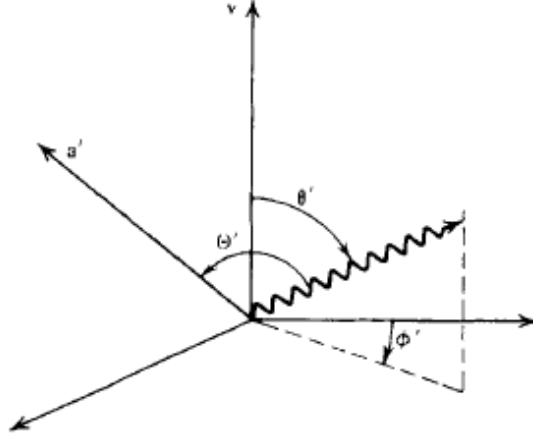
Figure 2.3: Geometry for dipole emission. (Source: Rybicki and Lightman)

It is clear from the figure that θ is the angle between the velocity vector and the field emitted whereas Θ is the angle between the acceleration vector and the direction of emission. Consider now, the following two cases:

- Case 1 - Acceleration $\parallel$ to Velocity:

$$\frac{dP_{\parallel}}{d\Omega} = \frac{q^2}{4\pi c^3} a_{\parallel}^2 \frac{sin^2\theta}{(1 - \beta cos\theta)} \tag{2.7}$$

- Case 2 - Acceleration $\perp$ to Velocity:

$$\frac{dP_{\perp}}{d\Omega} = \frac{q^2 a_{\perp}^2}{4\pi c^3} \frac{1}{(1 - \beta cos\theta)^4} \left[1 - \frac{sin^2\theta cos^2\phi}{\gamma^2 (1 - \beta cos\theta)^2} \right] \tag{2.8}$$

Figure 2.4 summarizes both the important cases concisely. It has again been taken from Rybicki & Lightman. It is important to note that radiation in both the cases is emitted at an angle $\theta \sim \frac{1}{\gamma}$ so that most of the radiation is concentrated in the forward direction and is confined to a narrow cone since γ is a large number. This is known as the *beaming effect*.

10
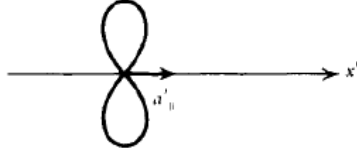
(a)

Dipole radiation pattern for particle at rest.

(b)

Angular distribution of radiation emitted by a particle with parallel acceleration and velocity.
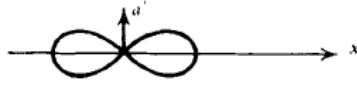
(c)

Same as a.

(d)

Angular distribution of radiation emitted by a particle with perpendicular acceleration and velocity.

Figure 2.4: Two important cases of Relativistic Beaming. (Source: Rybicki and Lightman)

In the extreme relativistic case, $\gamma >> 1$. The denominators in Equations 2.7 and 2.8 become very small and the radiation becomes strongly peaked in the forward direction. In this limit, we obtain the following complicated looking expressions for the above two cases:

$$\frac{dP_{\parallel}}{d\Omega} \approx \frac{16q^2 a_{\parallel}^2}{\pi c^3} \gamma^{10} \frac{\gamma^2 \theta^2}{(1 + \gamma^2 \theta^2)^6} \text{ and,} \tag{2.9}$$

$$\frac{dP_{\perp}}{d\Omega} \approx \frac{4q^2 a_{\perp}^2}{\pi c^3} \gamma^8 \left[\frac{1 - 2\gamma^2 \theta^2 cos2\phi + \gamma^4 \theta^4}{(1 + \gamma^2 \theta^2)^6} \right] \tag{2.10}$$

Even though these look intimidating, all we really need to note is that these expressions

11

depend on θ solely through the combination $\gamma\theta$. This shall be used in the subsequent section where we derive the standard model of particle spectra qualitatively.

Chapter 3

Qualitative Derivation of the Standard Model of Synchrotron Spectra

3.1 Synchrotron Spectra of a Single Electron

As we have seen, Larmor's formula contains the square of the acceleration of the particle. One can use the *Lorentz Force* law together with *Newton's Equations of Motion* to transform the perpendicular component of Equation 2.6 into the following form using $a_\perp = \omega_B v_\perp$ with $\omega_B = \dfrac{qB}{\gamma mc}$:

$$P = \frac{2}{3}r_0^2 c \beta_\perp^2 \gamma^2 B^2 \tag{3.1}$$

It should be noted that we are using the Guassian-CGS unit system in this derivation. We now need to average the above formula over all angles which makes sense for an isotropic distribution of velocities.

$$P_{avg} = \frac{2}{3}r_0^2 c \gamma^2 \frac{\beta^2}{4\pi}B^2 \int sin^2\alpha \, d\Omega = \frac{4}{3}\sigma_T c \beta^2 \gamma^2 U_B \tag{3.2}$$

Here $\sigma_T = 8\pi r_0^2/3$ is the classical Thomson cross- section and U_B is the magnetic field energy density. This final formula in equation 2.12 is a very important one and shall be used again for comparison in order to find the power emitted by a single electron as a function of frequency per unit frequency.

In order to proceed with the same, we first need to relate the synchrotron spectrum with the

variation of the electric field as seen by the observer as power is proportional to the square of the electric field (Equation 2.3). We shall also encounter the concept of *critical frequency* which shall serve as one of the most important quantities in the discussion followed.
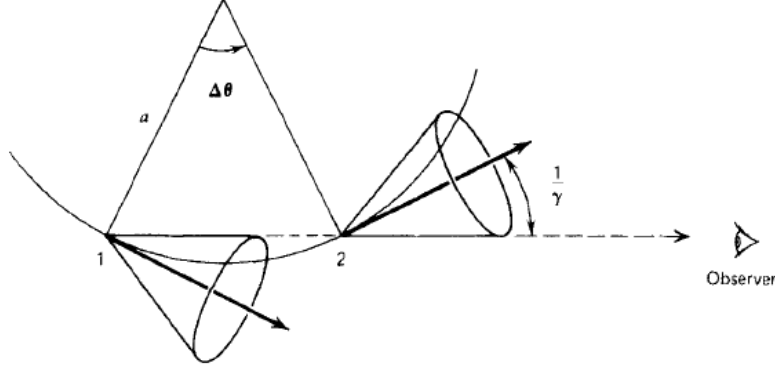
Figure 3.1: Emission cones at various points of an accelerated particle's trajectory. Picture taken from Rybicki & Lightman.

Consider the above diagram. The arc length $\triangle s$ is related to the radius of curvature of the path by $a = \triangle s/\triangle\theta$. Using the equation of motion,

$$\gamma m \frac{\triangle v}{\triangle t} = \frac{q}{c}(\mathbf{v} \times \mathbf{B})$$

and the fact that $|\triangle \mathbf{v}| = v\triangle\theta$ together with $\triangle s = v\triangle t$ gives the following results:

$$\frac{\triangle\theta}{\triangle s} = \frac{qB\sin\alpha}{\gamma mcv} \quad ; \quad a = \frac{v}{\omega_B \sin\alpha} \quad ; \quad \triangle s = \frac{2v}{\gamma\omega_B \sin\alpha}$$

Using all these and a few more algebraic manipulations, one can estimate the time difference between the emitted and received beams of radiation in the line of sight of the observer to be:

$$\triangle t^A \approx \left(\gamma^3 \omega_B \sin\alpha\right)^{-1}$$

The expression suggests that the width of the observed pulses is smaller than the gyration period by a factor γ^3. This in turn means that the spectrum will be fairly broad and cut-off at frequencies corresponding to the inverse of the above time period. Such a frequency is given a special name in the context of synchrotron radiation and is known as the **critical**

frequency. It depends on the square of the Lorentz factor γ, the magnetic field B and also the pitch angle α.

$$\omega_c \equiv \frac{3}{2}\gamma^3 \omega_B sin\,\alpha = \frac{3\gamma^2 q B sin\,\alpha}{2mc} \tag{3.3}$$

So far we have been only been developing the tools necessary for the qualitative derivation. It is clear that the power spectrum will extend to something of the order of the critical frequency before falling off. Making use of the fact that the electric field depends on θ solely through the combination $\gamma\theta$ (*The beaming effect*, Equations 2.9 and 2.10) lets us write $E(t) \propto F(\gamma\theta)$. One can further use a similar machinery as that used to find the critical frequency to find a relation between θ and time t.

$$\gamma\theta \approx 2\gamma \left(\gamma^2 \omega_B sin\,\alpha\right) t \propto \omega_c t \tag{3.4}$$

The time dependence of the electric field can now be written as, $E(t) \propto g(\omega_c t)$. However, what we need for finding the spectrum is the square of the Fourier transform of the electric field.

$$\hat{E}(\omega) \propto \int_{-\infty}^{\infty} g(\omega_c t)\, e^{i\omega t} dt \tag{3.5}$$

$$\frac{dW}{d\omega d\Omega} \propto \left|\hat{E}(\omega)\right|^2 = \left|\int_{-\infty}^{\infty} g(\omega_c t)\, e^{i\omega t} dt\right|^2 \tag{3.6}$$

One can mentally change the variables of integration to $\xi = \omega_c t$. This makes it clear that the integrand is now only a function of the quantity ω/ω_c. Integrating the power spectrum per unit frequency over the solid angle and dividing by the period of orbit (both independent of frequency), we get:

$$\frac{dW}{d\omega dt} = T^{-1}\frac{dW}{d\omega} \equiv P(\omega) = C_1 F\left(\frac{\omega}{\omega_c}\right) \tag{3.7}$$

This can now be integrated over all frequencies to get the total power radiated per unit frequency by a single electron.

$$P = \int_0^{\infty} P(\omega) d\omega = C_1 \int_0^{\infty} F\left(\frac{\omega}{\omega_c}\right) d\omega = \omega_c C_1 \int_0^{\infty} F\left(x\right) dx \tag{3.8}$$

Comparing it with our previous expression of average power (Equation 2.12), gives us for the highly relativistic case ($\beta \approx 1$), the power radiated per unit frequency as a function of frequency for a single synchrotron electron.

$$P(\omega) = \frac{\sqrt{3}e^3 B \sin\alpha}{8\pi^2 \epsilon_0 c m_e} F(x) \tag{3.9}$$

3.2 Synchrotron Spectra for a Power Law Distribution Function

We have already arrived at the expression for the power radiated by a single electron in a magnetic field. The next part is to figure out the total power radiated by a distribution of such electrons. Traditionally, the electron energy distribution function (DF) has been chosen to be a decaying power law with a high energy cut-off i.e. $N(\gamma)d\gamma = C\gamma^{-p}d\gamma$. The total emitted power by such a distribution of electrons will just be the integral over the particle energies:

$$P_{tot}(\omega) = C\int_{\gamma_1}^{\gamma_2} P(\omega)\gamma^{-p}d\gamma \propto \int_{\gamma_1}^{\gamma_2} F\left(\frac{\omega}{\omega_c}\right)\gamma^{-p}d\gamma \propto \omega^{-(p-1)/2}\int_{x_1}^{x_2} F(x)\, x^{(p-3)/2}dx \tag{3.10}$$

What makes the standard model standard is the following: if the energy limits are far too wide, one can approximate the limits as $x_1 \approx 0$ and $x_2 \approx \infty$. In that case, the integral is just a constant and we obtain the following well known expression:

$$P_{tot}(\omega) \propto \omega^{-(p-1)/2} \tag{3.11}$$

The spectral index s is related to the particle DF index p through

$$s = \frac{p-1}{2}$$

Arriving at this expression by invoking the above assumptions comes at its own cost. For one, the power appears to blow at $\omega = 0$. Such (and other) problems are solved when we look at things much more carefully. Working to solve this problem is one of the main aims of our MS-Thesis.

Chapter 4

Detailed derivation of the Synchrotron Spectrum using Lienard-Weichert Potentials

The derivation for the same is extremely technical and involved. We shall only present a short summary of it here for the sake of completeness. We shall be following Longair which uses the SI system of units.

4.1 Potentials and the Coordinate System

The expression for the radiation spectrum of a moving electron is:

$$\frac{dW}{d\omega d\Omega} = \frac{e^2}{16\pi^3\epsilon_0 c} \left| \int_{-\infty}^{+\infty} \left\{ \mathbf{n} \times \left[\left(\mathbf{n} - \frac{\mathbf{v}}{c} \right) \times \frac{\dot{\mathbf{v}}}{c} \right] \kappa^{-3} \right\}_{ret} exp(i\omega t)\, dt \right|^2 \qquad (4.1)$$

Here $\kappa = [1 - (\mathbf{v}\,.\,\mathbf{n})/c]$ and the vector $\mathbf{n}$ is the unit vector from the electron to the point of observation. It is possible to manipulate this complicated looking expression into a more manageable form for later use.

$$\frac{dW}{d\omega d\Omega} = \frac{e^2}{16\pi^3\epsilon_0 c} \left| \int_{-\infty}^{\infty} \mathbf{n} \times \left(\mathbf{n} \times \frac{\mathbf{v}}{c} \right) exp \left[i\omega \left(t' - \frac{\mathbf{n}\,.\,\mathbf{r_0}(t')}{c} \right) \right] dt \right|^2 \qquad (4.2)$$

This form does not include the acceleration of the particle and only the dynamics of the electron appear hereon. The next part of setting the stage involves setting up a proper coordinate system for the problem. The reader might find it useful to refer to the following

diagram:
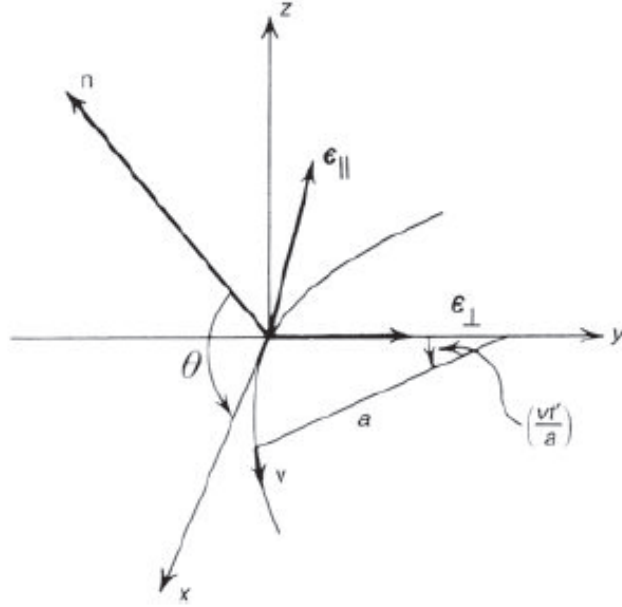
Figure 4.1: Coordinate system for evaluating the Intensity of synchrotron radiation. (Source: Longair)

The vector $\mathbf{n}$ points from the electron to the observer as mentioned before and is taken to lie in the $x - z$ plane. We define a vector $\epsilon_{\|}$ lying in the plane containing the vector $\mathbf{n}$ and the magnetic field. We also define a vector $\epsilon_{\perp}$ that lies along the y-axis. These three vectors $\mathbf{n}$, $\epsilon_{\|}$ and $\epsilon_{\perp}$ form a natural system of linearly independent vectors. The parallel and perpendicular directions are with regard to the direction of the magnetic field as seen by the observer.

4.2 The Algebra

We consider the coordinates of the electron in the $(\mathbf{n}, \epsilon_{\|}, \epsilon_{\perp})$ coordinate system such that $t' = 0$ at $x = y = z = 0$. After a time t', the electron will have moved a distance vt' and the angle it would have swept would be $\phi = vt'/a$. From figure 4.1:

$$\mathbf{v} = |\mathbf{v}| \left[i_x cos \left(\frac{vt'}{a} \right) + \epsilon_{\perp} sin \left(\frac{vt'}{a} \right) \right] \tag{4.3}$$

18

The first term in the square bracket can be decomposed in terms of the vectors ($\mathbf{n}$ and $\epsilon_\parallel$):

$$\mathbf{v} = |\mathbf{v}| \left[\epsilon_\perp sin\left(\frac{vt'}{a}\right) + \mathbf{n}cos\,\theta\,cos\left(\frac{vt'}{a}\right) - \epsilon_\parallel sin\,\theta\,cos\left(\frac{vt'}{a}\right) \right] \tag{4.4}$$

We can now compute the vector triple product $\mathbf{n} \times (\mathbf{n} \times \mathbf{v})$ in Equation 4.2 remembering that $\mathbf{n} \times \epsilon_\perp = \epsilon_\parallel$ and $\mathbf{n} \times \epsilon_\parallel = -\epsilon_\perp$. The first term in 4.2 simplifies to:

$$\mathbf{n} \times (\mathbf{n} \times \mathbf{v}) = |\mathbf{v}| \left[-sin\left(\frac{vt'}{a}\right)\epsilon_\perp + sin\,\theta\,cos\left(\frac{vt'}{a}\right)\epsilon_\parallel \right] \tag{4.5}$$

To evaluate the exponent in 4.2, we need to put in the value of $\mathbf{r_0}(t')$. We shall not show its complete expression here for the sake of being concise. It should, however, be noted that the term in the exponent simplifies greatly.

$$\left[t' - \frac{\mathbf{n}.\mathbf{r_0}(t')}{c} \right] = t' - \frac{a}{c}cos\,\theta\,sin\left(\frac{vt'}{a}\right) \tag{4.6}$$

One can now use the small angle approximations for $sin\left(\frac{vt'}{a}\right)$ and $cos\,\theta$ as the largest contributions in the exponent come from small values of $[t' - \mathbf{n}.\mathbf{r_0}(t')/c]$. Otherwise, there would be many 'oscillations' in the integral and the overall value would turn out to be very small. This is precisely why using the small angle approximation for these trigonometric functions is justified. In this case, it is enough to expand them to 3rd order in their respective arguments.

$$t' - \frac{\mathbf{n}.\mathbf{r_0}(t')}{c} \approx \frac{1}{2\gamma^2} \left[t'(1 + \gamma^2\theta^2) + \frac{c^2\gamma^2 t'^3}{3a^2} \right] \tag{4.7}$$

We next make small angle approximations in the expression for the vector triple product as well:

$$\mathbf{n} \times (\mathbf{n} \times \frac{\mathbf{v}}{c}) = \left|\frac{\mathbf{v}}{c}\right| \left[-sin\left(\frac{vt'}{a}\right)\epsilon_\perp + sin\,\theta\,cos\left(\frac{vt'}{a}\right)\epsilon_\parallel \right] \approx \left(\frac{-vt'}{a}\epsilon_\perp + \theta\epsilon_\parallel \right) \tag{4.8}$$

All this effort can now be utilized in writing down the power separately in the $\epsilon_\parallel$ and $\epsilon_\perp$ directions.

$$\frac{dW_\perp(\omega)}{d\omega d\Omega} = \frac{e^2\omega^2}{16\pi^3\epsilon_0 c} \left| \int_{-\infty}^{\infty} \frac{vt'}{a} exp\left\{ \frac{i\omega}{2\gamma^2} \left[t'(1 + \gamma^2\theta^2) + \frac{c^2\gamma^2}{3a^2}t'^3 \right] \right\} dt' \right|^2 \tag{4.9}$$

$$\frac{dW_\parallel(\omega)}{d\omega d\Omega} = \frac{e^2\omega^2\theta^2}{16\pi^3\epsilon_0 c} \left| \int_{-\infty}^{\infty} exp\left\{ \frac{i\omega}{2\gamma^2} \left[t'(1 + \gamma^2\theta^2) + \frac{c^2\gamma^2}{3a^2}t'^3 \right] \right\} dt' \right|^2 \tag{4.10}$$

19

Taking the limits of the integral from $-\infty$ to ∞ is permissible because most of the power emitted by a synchrotron electron lies within small values of θ. In other words, since only a small section of values of t' corresponding to small values of θ contribute to the integral, there is little error in extending the limits from $-\infty$ to ∞.

The next part of the derivation in mostly changing variables and using the fact that these above integrals can be expressed in terms of modified Bessel functions of the 2nd kind. It suffices to say that Equations 4.9 and 4.10 reduce to:

$$\frac{dW_\perp(\omega)}{d\omega d\Omega} = \frac{e^2\omega^2}{12\pi^3\epsilon_0 c}\left(\frac{a\theta_\gamma}{c\gamma^2}\right)^2 K_{2/3}^2(\eta) \tag{4.11}$$

$$\frac{dW_\parallel(\omega)}{d\omega d\Omega} = \frac{e^2\omega^2\theta^2}{12\pi^3\epsilon_0 c}\left(\frac{a\theta_\gamma}{c\gamma}\right)^2 K_{1/3}^2(\eta) \tag{4.12}$$

Here $\theta_\gamma^2 = (1 + \gamma^2\theta^2)$ and $\eta = \omega a\theta_\gamma^3/3c\gamma^3$. Finally, we need to integrate over the angle θ the details of which can be found in Westfold's 1959 paper. It is traditional to write:

$$\mathrm{F}(x) = x\int_x^\infty K_{5/3}(z)\,dz \tag{4.13a}$$

$$\mathrm{G}(x) = xK_{2/3}(x) \tag{4.13b}$$

We finally arrive at the following nice looking set of equations:

$$\frac{dW_\perp(\omega)}{d\omega} = \frac{\sqrt{3}e^2\gamma\sin\alpha}{8\pi\epsilon_0 c}[F(x) + G(x)] \tag{4.14}$$

$$\frac{dW_\parallel(\omega)}{d\omega} = \frac{\sqrt{3}e^2\gamma\sin\alpha}{8\pi\epsilon_0 c}[F(x) - G(x)] \tag{4.15}$$

The net power per unit frequency as a function of frequency is just the sum of the powers in the two perpendicular directions. Summing 4.13 and 4.14 yields a result very similar to Equation 3.9 that was obtained merely through qualitative discussions.

$$\frac{dW(\omega)}{d\omega} = \frac{\sqrt{3}e^2\gamma\sin\alpha}{8\pi\epsilon_0 c}F(x) \tag{4.16}$$

20

4.3 The Synchrotron Radiation of a Power Law Distribution of Electron Energies

To obtain the frequency integrated emission, or emission from a power law distribution of electrons, we need to have the integrals over the F and G functions. One may use the following derived relations from Abramowitz and Stegun given in Rybicki and Lightman:

$$\int_0^\infty x^\mu F(x)\, dx = \frac{2^{\mu+1}}{\mu+2}\Gamma\left(\frac{\mu}{2}+\frac{7}{3}\right)\Gamma\left(\frac{\mu}{2}+\frac{2}{3}\right) \tag{4.17a}$$

$$\int_0^\infty x^\mu G(x)\, dx = 2^\mu\Gamma\left(\frac{\mu}{2}+\frac{4}{3}\right)\Gamma\left(\frac{\mu}{2}+\frac{2}{3}\right) \tag{4.17b}$$

In order to evaluate the total power emitted by a distribution of electrons, all we need to do now is integrate Equation 4.15 using Equation 4.16a. This shall make use of the fact that $\mu = (p-3)/2$. The final expression for *total power per unit frequency* as a function of frequency from a *power law distribution* of electron energies, $N(E)\, dE = \kappa E^{-p} dE$ is given by:

$$P_{tot}(\omega) = \frac{\sqrt{3}e^3 B\kappa \sin\alpha}{8\pi^2\epsilon_0 c m_e(p+1)}\left(\frac{\omega m_e^3 c^4}{3eB\sin\alpha}\right)^{-(p-1)/2}\Gamma\left(\frac{p}{4}+\frac{19}{12}\right)\Gamma\left(\frac{p}{4}-\frac{1}{12}\right) \tag{4.18}$$

Chapter 5

Filamentary Magnetic Fields

5.1   The Model

Now that the theory of the standard model of synchrotron spectra has been developed, we need to see how well can it be applied to real life scenarios, like hotspots or lobes of radio galaxies. However, as **Eilek and Arendt 1996** point out, the standard model is overly restrictive and a little too naive, especially in applications to spectral aging of radio sources, working on which is after all, a major aim of our MS-thesis.

Summarizing the standard model, the reader shall remember that the synchrotron spectrum depends upon the particle energy E (or equivalently γ) and the magnetic field B. The magnetic field is taken to be homogeneous and constant throughout the source which is a rather weak assumption when it comes to space plasmas or even plasmas in laboratories.

As our interferometers have become better at resolving far away sources, filamentary nature of magnetic fields has turned up from time to time. The exact reason for their existence might not be known as of now but they could be in part due to fluctuations in magnetic fields at the intermediate scales (Eilek and Arendt 1996). Thus, any realistic model should incorporate these kinds of substructures/magnetic field distributions throughtout the emitting volume.

For purposes relevant to us, we imagine several filaments of strong magnetic field strengths immersed in a background region of plasma and gas where the field is much weaker. The salient features of our model are:

- The gyroradius r of the electron's trajectory is the related to the Lorentz factor γ and

the magnetic field B by:

$$r = \frac{\gamma mc}{eB \sin \alpha} \tag{5.1}$$

We note that the maximum possible gyroradius of the electron must equal the width/diameter l of a filament. This is just twice the gyroradius:

$$l = \frac{2\gamma mc}{eB \sin \alpha} \tag{5.2}$$

This equation relates the width of the filament, the magnetic field and the Lorentz factor of the synchrotron electron. We call this the *confinement condition*. Clearly r cannot exceed l if the electron has to reside inside the filament.

- In a steady state situation, there is a natural limit on r, namely the size of the filament. This in turn puts an upper limit on the value of the Lorentz factor (γ_{max}) given a particular value of the magnetic field B. This also means that if the $\gamma > \gamma_{max}$, the electron will be forced to reside outside the filament.

- Due to the inclusion of an upper limit, the integral limits can neither be extended artificially from 0 to ∞, nor can the P_{tot} integral be obtained analytically in closed form. The standard power law form of the synchrotron spectrum might get altered.

5.2   Numerical Analysis: An Approximation for the Bessel function Integral

The asymptotic forms of the function $F(x)$ from Rybicki and Lightman are as follows:

$$F(x) = \begin{cases} \frac{4\pi \sqrt[3]{\frac{x}{2}}}{\sqrt{3}\Gamma\left(\frac{1}{3}\right)} & x << 1 \quad (i) \\ \sqrt{\frac{\pi}{2}}e^{-x}\sqrt{x} & x >> 1 \quad (ii) \end{cases} \tag{5.3}$$

The reader is urged to recall that $x = \omega/\omega_c$ where ω_c is the critical frequency of the electron. We already had the asymptotic forms of the function but wanted to make it more precise. To achieve the same, we wrote a code in Mathematica and carried out a number of procedures to arrive at an approximate function $F_{apprx.}$:

- We first plotted $F(x)$ or the Bessel function integral (Equation 4.13a) numerically.

- Realizing that the shape could be obtained by multiplying an increasing function with a rapidly decreasing one, we took the functions in question to be a power law and a decaying exponential with arbitrary parameters.

- We then fit these to the original curve and figured out the values of the arbitrary parameters. To make things even more precise and accurate, we demanded that the percentage error be $< 5\%$ for all values of x.

- Making the above demand split the approximate function into 4 parts. The forms for $x << 1$ and $x >> 1$ were kept the same. The exact form for $F_{apprx.}$ is given below. Furthermore, we present various graphs to help the reader understand this function and its manufacturing procedure a little better.

$$
F_{apprx.}(x) = \begin{cases} \frac{4\pi \sqrt[3]{\frac{x}{2}}}{\sqrt{3}\Gamma\left(\frac{1}{3}\right)} & 0 < x < 0.0075 \quad (i) \\[3em] 1.761e^{-x}x^{0.291} & 0.0075 \le x < 1 \quad (ii) \\[3em] e^{-x}\left(1.07x^{0.513} + 0.701\right) & 1 \le x < 26 \quad (iii) \\[3em] \sqrt{\frac{\pi}{2}}e^{-x}\sqrt{x} & x \ge 26 \quad (iv) \end{cases}
\tag{5.4}
$$

The % error with respect to an approximate form $Y(x)$ of the Bessel function integral $F(x)$ as a function of x is given below. $Y(x)$ can be any one of the equations 5.3 and 5.4 depending upon which one of them is required.

$$
\% \text{ error w.r.t Y(x)} = \left| \left(\frac{x\int_x^\infty K_{\frac{5}{3}}(\xi)d\xi - \text{apprx. form Y(x) of } F(x)}{x\int_x^\infty K_{\frac{5}{3}}(\xi)d\xi} \right) \times 100 \right|
\tag{5.5}
$$

24
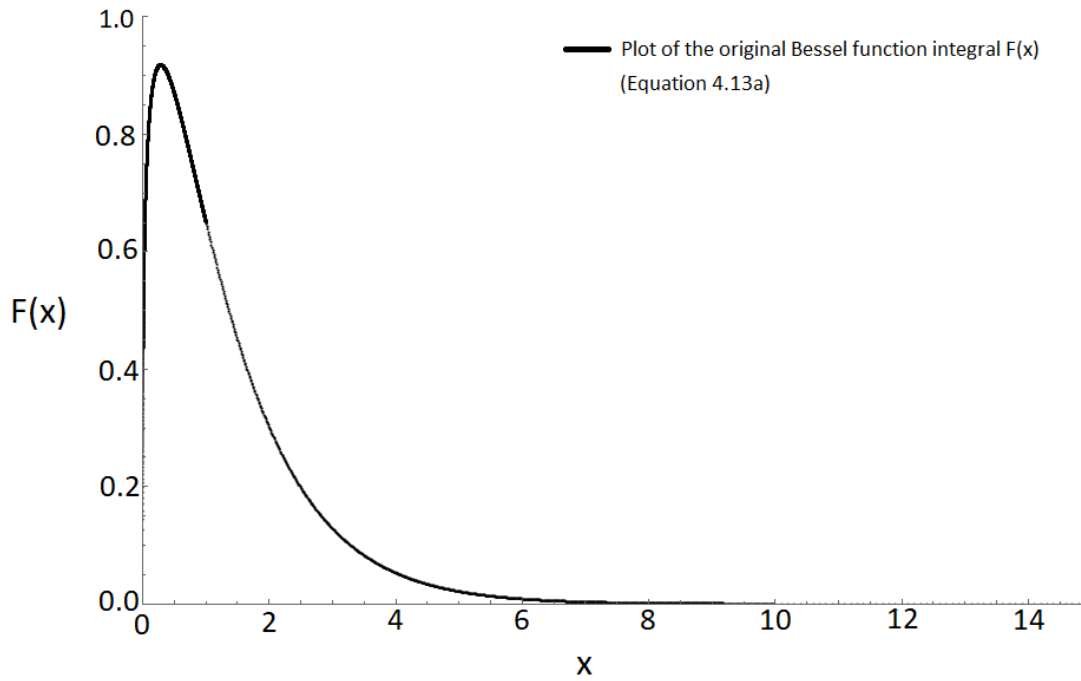
Figure 5.1: The original Bessel function integral $F(x)$, Equation 4.13a
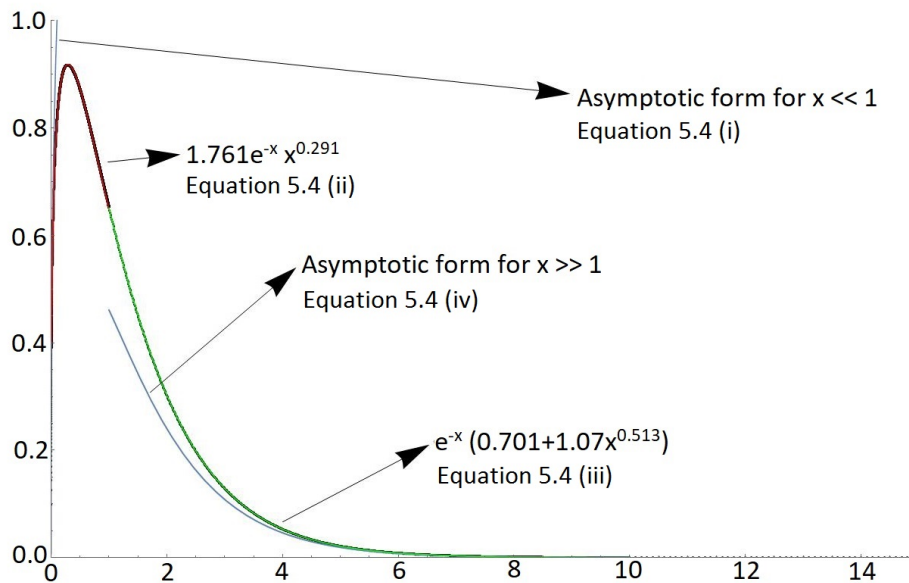
Figure 5.2: $F_{apprx.}(x)$ (Equation 5.4) superimposed on $F(x)$ (Equation 4.13a)

25
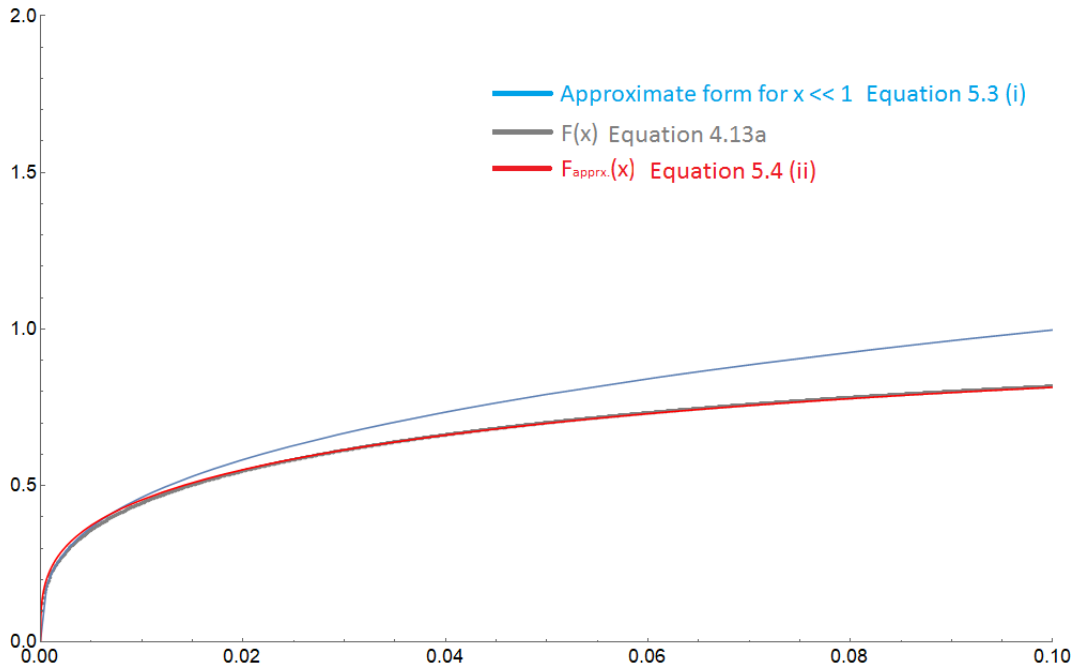
Figure 5.3: $F(x)$ (Eqn. 4.13a), $F_{apprx.}(x)$ (Eqn. 5.4 (ii)) and the asymptotic form for $x << 1$ (Eqn. 5.3 (i))
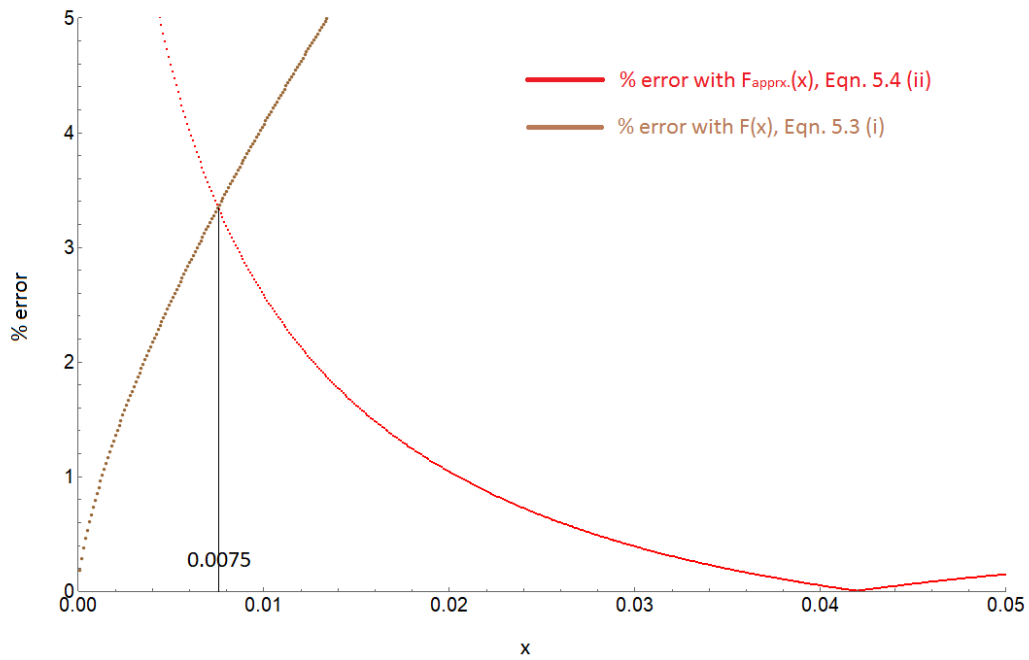
Figure 5.4: % error between $F(x)$ (Eqn. 4.13a) and $F_{apprx.}(x)$ (Eqn. 5.4 (ii)) and $x << 1$ asymptotic form of $F(x)$ (Eqn. 5.3 (i))
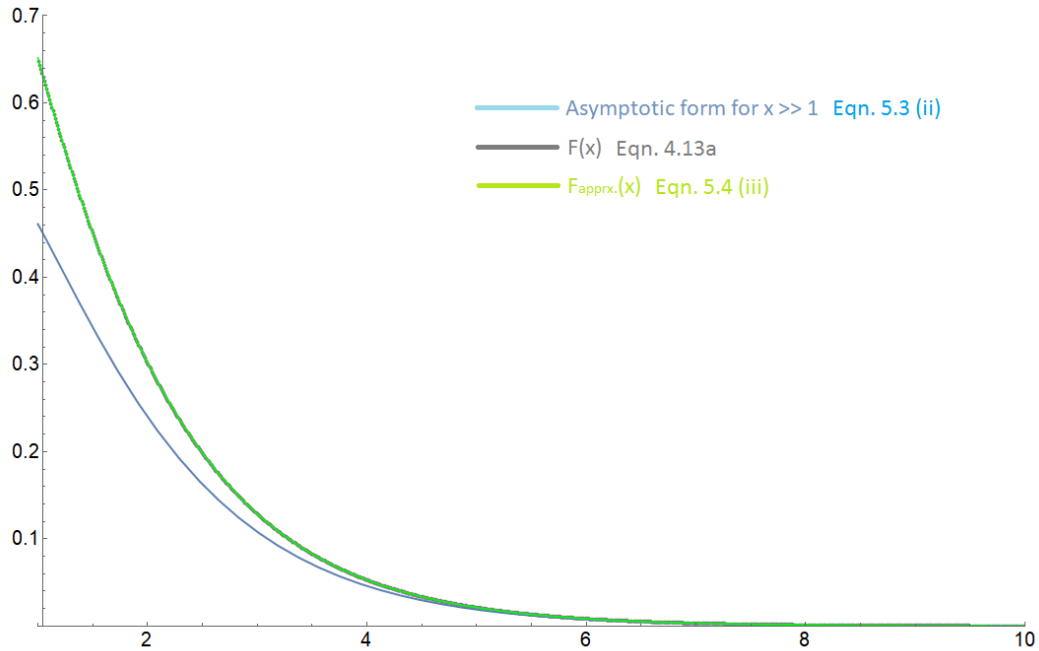
Figure 5.5: $F(x)$ (Eqn. 4.13a), $F_{apprx.}(x)$ (Eqn. 5.4 (iii)) and the asymptotic form for $x >> 1$ (Eqn. 5.3 (ii))
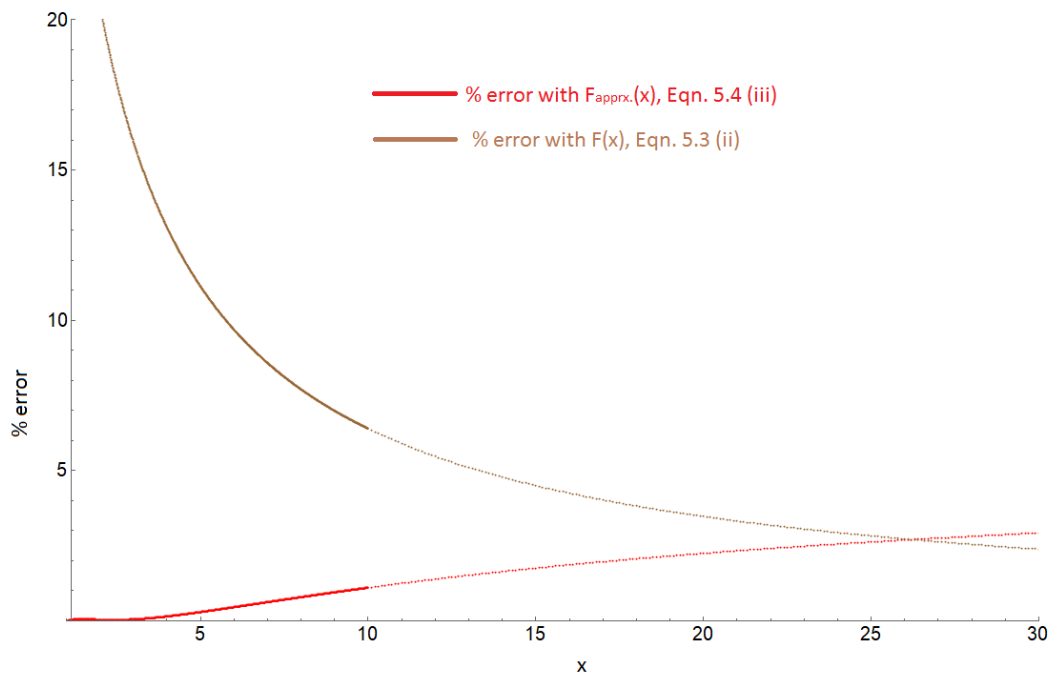
Figure 5.6: % error between $F(x)$ (Eqn. 4.13a) and $F_{apprx.}(x)$ (Eqn. 5.4 (iii)) and $x << 1$ asymptotic form of $F(x)$ (Eqn. 5.3 (ii))

5.3 Checks made using $F_{apprx.}(x)$

The overall constants modulo physical quantities like electric charge, magnetic field, mass of the electron and speed of light etc. in the original and approximate expressions of total power are respectively:

$$\frac{1}{(p+1)}\Gamma\left(\frac{p}{4}+\frac{19}{12}\right)\Gamma\left(\frac{p}{4}-\frac{1}{12}\right) \tag{5.6a}$$

$$2^{\frac{-(p+1)}{2}}\int_0^\infty F_{apprx.}(x)\,dx \tag{5.6b}$$

The following table compares these values for three different values of the power law distribution index p. The middle column gives the value of the power integral constant calculated through $F(x)$ (Eqn. 4.13a) while the rightmost one gives it for the constant calculated through $F_{apprx.}(x)$ (Eqn. 5.4). One notes that the values of the two constants are very close and quite insensitive to the value of p.

Value of p	Original Function $F(x)$	Approximate Function $F_{apprx.}(x)$
5	0.266648	0.266409
6	0.273897	0.273557
7	0.313496	0.312980

Table 5.1: Comparison of constants for different values of p

Although the % error seems to increase, we need not worry about it as the values of spectral index s rarely turn out to be above 3. That means at max, a % error of 0.16 in the value of the constant calculated through $F_{apprx.}(x)$.

5.4 Log-Log Plots of Power Vs. Frequency

After checking the value of the overall constant, the next step was to actually plot things. We plotted power vs. frequency plots for a wide set of parameters B, p and γ_{max} and the results were in accordance with the work of **Eilek and Arendt (1994)**.
In particular, we took the magnetic field to be of the order of a few hundred Tesla (**Carilli 1999**), varied the value of γ_{max} over three orders of magnitude and also changed the DF parameter p to see how the spectrum got effected.

We shall not be presenting all these cases here. Instead, we shall show only one of the plots and then list out all the general results that we extracted out of this exercise. In particular. we show the graph for the case $B = 10^{-7}$ T, $p = 5$ and $\gamma_{max} = 100$.
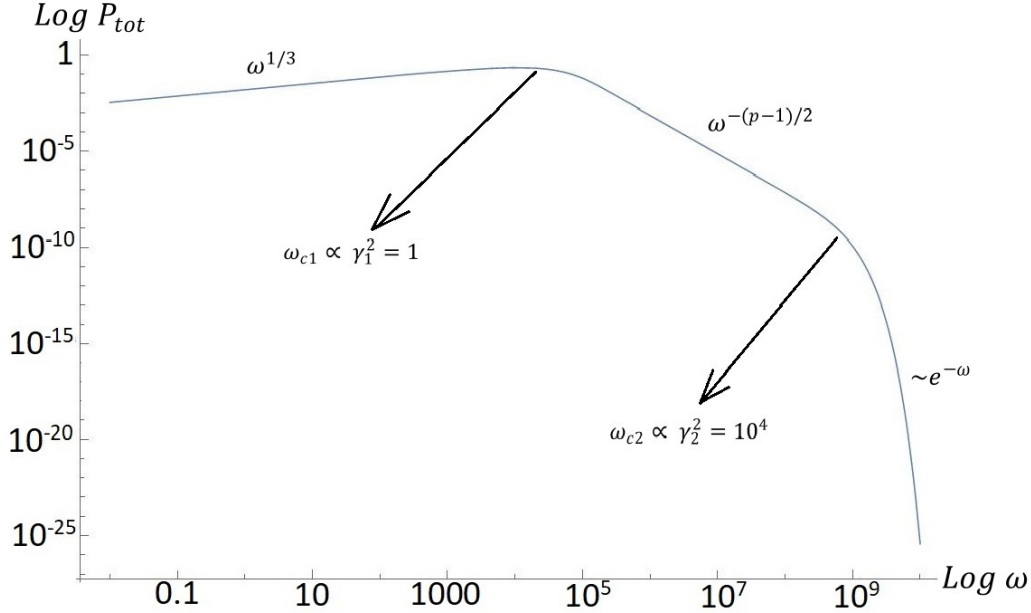
Figure 5.7: Log-Log plot showing synchrotron power P as a function of frequency ω. Here, $B = 10^{-7}$ T, $p = 5$ and $\gamma_{max} = 100$.

The notable points deduced from all this hard work are as follows:

- The slope of the increasing part turned out to be $1/3$ in all the cases irrespective of the values of B, p or γ_{max}.

- The middle part follows the standard power law dependence i.e. $P_{tot}(\omega) \propto \omega^{-(p-1)/2}$.

- The rapidly decreasing part is not a straight line on log-log scale and was verified to be an exponential cut-off.

- The trends seen in the above curves can be easily explained just by staring at the expression for the critical frequency.

- To recall, $\omega_{sy} = 26.4 \times 10^{10} \gamma^2 B$ Hz in SI units.

- The curves turn at two fiducial frequencies: ω_0 corresponding to $\gamma = 1$ and ω_c corresponding to $\gamma = \gamma_{max}$.

- The slope $1/3$ occurs for $\omega << \omega_0$ while the spectrum cuts off exponentially at high frequencies when $\omega >> \omega_c$.

It was further found that ω_{sy} doesn't depend on p which makes sense as ω_c doesn't have any p dependence. We also verified that the magnetic field B indeed follows a linear trend while for γ_{max} the trend is quadratic. In other words, the turn-over frequencies, ω_{c1} and ω_{c2} are independent of the values of the power law distribution index (p). $\omega_{c1} \propto \gamma_1^2$ whereas $\omega_{c2} \propto \gamma_2^2$ and the $\omega_c \propto \gamma^2 B$ trend was also verified.

Chapter 6

The Pressure Balance Equation

All our analysis so far has been without any regard to filaments. But it guarantees the fact that our code and analysis is correct by being concurrent with the work of Eilek and Arendt (1996). The next part in the puzzle is to actually invoke filaments and after that, distributions of filament sizes and magnetic fields and individually sum up the radiations coming from the filaments and the background. We start off with setting up the *pressure balance equation* for a single filament immersed in a weak background region of plasma.

6.1 Magnetic and Particle Pressures

A uniform magnetic field of strength B corresponds to a magnetic field energy density $B^2/2\mu_o$. This is true for both the filament as well as the background as long as the fields are constant and homogeneous. We also have pressure coming due to the relativistic motion of electrons. An electron with Lorentz factor γ has total energy equal to γmc^2. Multiplying this with the DF for particle energy, that has the dimensions of per unit volume, gives us the total particle pressure due to the relativistic kinematic motion of the electrons. For a single filament, the pressure balance equation then becomes (assuming constant magnetic fields both inside and outside the filament):

$$\frac{B_{in}^2}{2\mu_o} + \int_1^{\gamma_{max}} \gamma mc^2 K_{in}\gamma^{-p}\mathrm{d}\gamma = \frac{B_{out}^2}{2\mu_o} + \int_{\gamma_{max}}^{\infty} \gamma mc^2 K_{out}\gamma^{-p}\mathrm{d}\gamma \qquad (6.1)$$

Here $N(\gamma)d\gamma = K\gamma^{-p}d\gamma$ is the particle energy DF with dimensions of per unit volume. Equivalently, we may also express the same as $N(E)dE = K'E^{-p}dE$ but now $N(E)$ is the number density per unit energy of the synchrotron electrons.

6.2 The Single Filament Case

A single cylindrical filament of a finite radius is imagined to be immersed in a background region having a magnetic field much weaker than what's inside. The values of magnetic fields are taken to be constants so that the pressure balance equation takes a simple form. We also emphasize that this derivation is without invoking the minimum energy argument. We've tried to keep all physical quantities and expressions in SI units. The following cartoonish diagram might be helpful for the purposes of visualization.
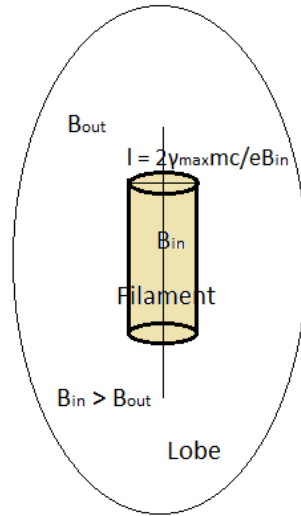
Figure 6.1: A rough sketch of a single filament immersed in a background region of plasma.

6.2.1 Independent Parameters

There are 4 independent parameters. These are: magnetic field inside the filament (B_{in}), width of the filament (l), contrast ratio between the fields $(\zeta = B_{out}/B_{in})$ and contrast ratio for the number densities $(k = n_{out}/n_{in})$.

6.2.2 The Contrast Ratio

For a constant magnetic field B, the magnetic field pressure is simply $\frac{B^2}{2\mu_0}$. Similarly, a population of relativistic electrons with a given number density will also contribute to pressure. In a state of equilibrium between the filament and the background, we can write the pressure

balance equation (it is again emphasized that the magnetic fields are constant) as follows:

$$\frac{B_{in}^2}{2\mu_o} + \int_1^{\gamma_{max}} \gamma mc^2 K_{in}\gamma^{-p}\mathrm{d}\gamma = \frac{B_{out}^2}{2\mu_o} + \int_{\gamma_{max}}^{\infty} \gamma mc^2 K_{out}\gamma^{-p}\mathrm{d}\gamma \tag{6.2}$$

Using the fact that $p > 5$, we can reduce the above equation to:

$$B_{out} = \sqrt{B_{in}^2 + \frac{2\mu_0 K_{in}mc^2}{3} - \frac{2\mu_0 mc^2(K_{in} + K_{out})}{3\gamma_{max}^3}} \tag{6.3}$$

We can then use the fact that K_1 and K_2 are related to n_1 and n_2 through number density integrals. From there we obtain the relations;

$$K_{in} = \frac{n_1(-p+1)}{\gamma_{max}^{-p+1}-1} \quad and \quad K_{out} = \frac{-n_2(-p+1)}{\gamma_{max}^{-p+1}} \tag{6.4}$$

Since $\gamma_{max} = \frac{leB}{2mc}$, and $\gamma_{max} >> 1$, we can neglect its inverse when being added to a considerably bigger quantity. After using this assumption and using the expression for K_{in} and K_{out} and rearranging the above equation, we finally obtain an equation relating ζ, p, k and l or equivalently, γ_{max}:

$$\zeta = \left(1 - \frac{2\mu_0 mc^2}{B_{in}^2}\left(\frac{1-p}{2-p}\right)\left[n_{out}\left(\frac{leB_{in}}{2mc}\right) - n_{in}\right]\right)^{1/2} \tag{6.5}$$

6.2.3 Filament

The total power per unit frequency as a function of frequency emitted only from the filament can be evaluated as:

$$P_{tot,fil} = \frac{\sqrt{3}e^3 B_{in}sin\alpha}{8\pi^2\epsilon_0 cm} \int_{\gamma=1}^{\gamma=\frac{leB_{in}}{2mc}} K_{in}F(\omega,\gamma,B_{in})\gamma^{-p}\mathrm{d}\gamma$$

$$= \frac{-n_{in}(-p+1)\sqrt{3}e^3 B_{in}\sin\alpha}{8\pi^2\epsilon_0 cm} \int_{\gamma=1}^{\gamma=\frac{leB_{in}}{2mc}} F(\omega,\gamma,B_{in})\gamma^{-p}\mathrm{d}\gamma \tag{6.6}$$

6.2.4 Background

To evaluate the total power per unit frequency emitted from only the background region, we need to evaluate the power integral with limits from γ_{max} to ∞. It is, however, very

important to note that the high frequency exponential cut-off emerges when the upper limit has a finite value, as needs to be done in a numerical treatment. Thus analytically, the expression for background radiation is:

$$P_{tot,bkg} = \frac{\sqrt{3}e^3 B_{out} sin\alpha}{8\pi^2 \epsilon_0 cm} \int\limits_{\gamma=\frac{leB_{in}}{2mc}}^{\gamma=\infty} K_{out} F(\omega, \gamma, B_{out}) \gamma^{-p} \mathsf{d}\gamma$$

After using the contrast ratio equations for the magnetic fields and the number densities, we can write the same as:

$$P_{tot,bkg} = \frac{-n_{in}(-p+1)\sqrt{3}e^3 \zeta B_{in} k sin\alpha}{8\pi^2 \epsilon_0 cm} \left(\frac{leB_{in}}{2mc}\right)^{p-1} \left[\int\limits_{\gamma=\frac{leB_{in}}{2mc}}^{\gamma=\infty} F(\omega, \gamma, B_{out}) \gamma^{-p} \mathsf{d}\gamma \right] \quad (6.7)$$

6.2.5   Sum of Synchrotron Radiation from the two regions

Most of the work is now done and all we now need to do is just manually add up the radiation from the filament and the background. We denote the sum simply by P_{tot} without any other subscript.

$$P_{tot} = \left(\frac{-n_{in}(-p+1)\sqrt{3}e^3 B_{in} sin\alpha}{8\pi^2 \epsilon_0 cm} \int\limits_{\gamma=1}^{\gamma=\frac{leB}{2mc}} F(\omega, \gamma, B_{out}) \gamma^{-p} \mathsf{d}\gamma \right) +$$

$$\left(\frac{-n_{in}(-p+1)\sqrt{3}e^3 \zeta B_{in} k sin\alpha}{8\pi^2 \epsilon_0 cm} \left(\frac{leB_{in}}{2mc}\right)^{p-1} \int\limits_{\gamma=\frac{leB}{2mc}}^{\gamma=\infty} F(\omega, \gamma, B_{out}) \gamma^{-p} \mathsf{d}\gamma \right)$$

Many of the terms can be taken common and the simplified expression (Equation (7)) can be written down as:

$$P_{tot} = \frac{-n_{in}(-p+1)\sqrt{3}e^3 B_{in} sin\alpha}{8\pi^2 \epsilon_0 cm} \left\{ \int\limits_{\gamma=1}^{\gamma=\frac{leB_{in}}{2mc}} F(\omega, \gamma, B_{in}) \gamma^{-p} \mathsf{d}\gamma + k\zeta \left(\frac{leB_{in}}{2mc}\right)^{p-1} \int\limits_{\gamma=\frac{leB_{in}}{2mc}}^{\gamma=\infty} F(\omega, \gamma, \zeta B_{in}) \gamma^{-p} \mathsf{d}\gamma \right\}$$

As can be seen, (7) contains only four independent parameters: B_{in}, ζ, k and width of the

filament l.

6.2.6   Mathematica code Summary

In our Mathematica code, we took solid values for each of the independent parameters. We then solved (4) for the number density (n_{in}) which means we also have n_{out} since we only need to multiply the former by k. It should be mentioned that presence of a single filament did not change the spectrum in any major way, although it does look significantly different from that of a uniform field region case. This was enough motivation for us to move forward and do the two (many) filament region case. In the following graph, we compare the uniform field spectrum with that of the composite spectrum of a single filament + background. The values of the contrast ratio parameters ζ and k have been chosen to be approximately equal to 1.
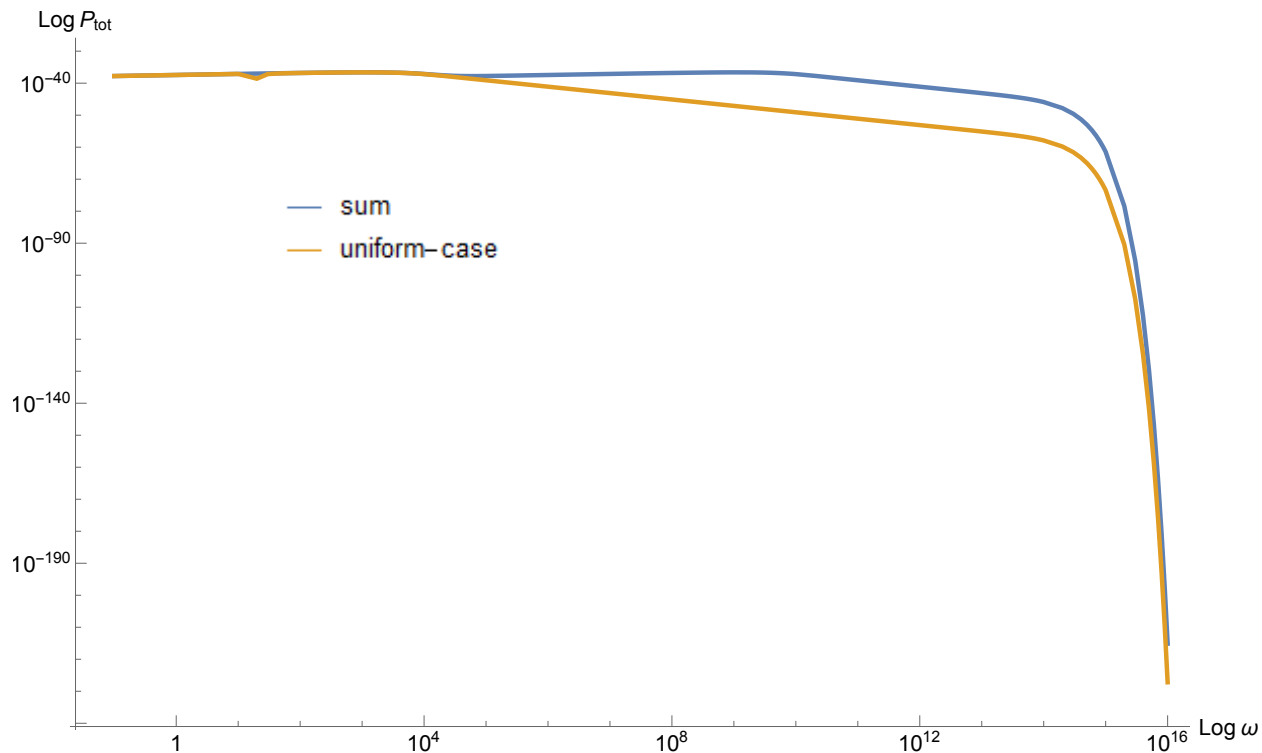

Figure 6.2: Uniform field case Vs. Composite spectrum with $\zeta = 0.999$ and $k = 0.999$.

Even though the break-frequencies roughly match in the two cases, there is significant deviation from the uniform magnetic field case. This is enough motivation for the fact that the incorporation of filaments in an otherwise uniform magnetic field region can cause extra

35

break-frequencies to appear. This phenomenon is closely tied together with the concept of *synchrotron aging* and shall be talked about in further detail with regard to the two filament-region case.

6.2.7 Sensitivity Analysis

In order to find out how sensitive each independent parameter is, we plotted several curves for each parameter while keeping the value of the other three parameters constant (at some reference value). This allowed us to figure out the break-frequencies with respect to each of the independent parameters. We have presented the graphs as well as % error plots for each of the independent parameter below and have also tried to provide a concise explanation of the trend seen. We frequently use the term % error in the following sections. We define it for an arbitrary parameter X (as a function of the frequency ω) in the following manner:

$$\% \text{ error } (\omega) = \left| \left(\frac{P_{tot}(\omega) \text{ for reference value of X} - P_{tot}(\omega) \text{ for some other value of X}}{P_{tot}(\omega) \text{ for reference value of X}} \right) \times 100 \right|$$

$$(6.8)$$

Magnetic Field B

We present Log-Log plot of synchrotron power vs. frequency ω for two values of B, $B = 10^{-8}$ T (reference) and $B = 10^{-7}$ T. We can clearly see the 4 break frequencies. Here we have taken $\zeta = 0.999$, $k = 0.999$ and $\gamma_{max} = 10^3$. The trend that the critical frequency ω_c for a composite spectrum depends linearly on B is also verified. The second plot is a Log-Log plot of the percentage error vs. frequency ω again for $B = 10^{-8}$ T and $B = 10^{-7}$ T. This plot shows that B_{in} is an extremely sensitive parameter especially at high frequencies ($> 10^{13}$ Hz).
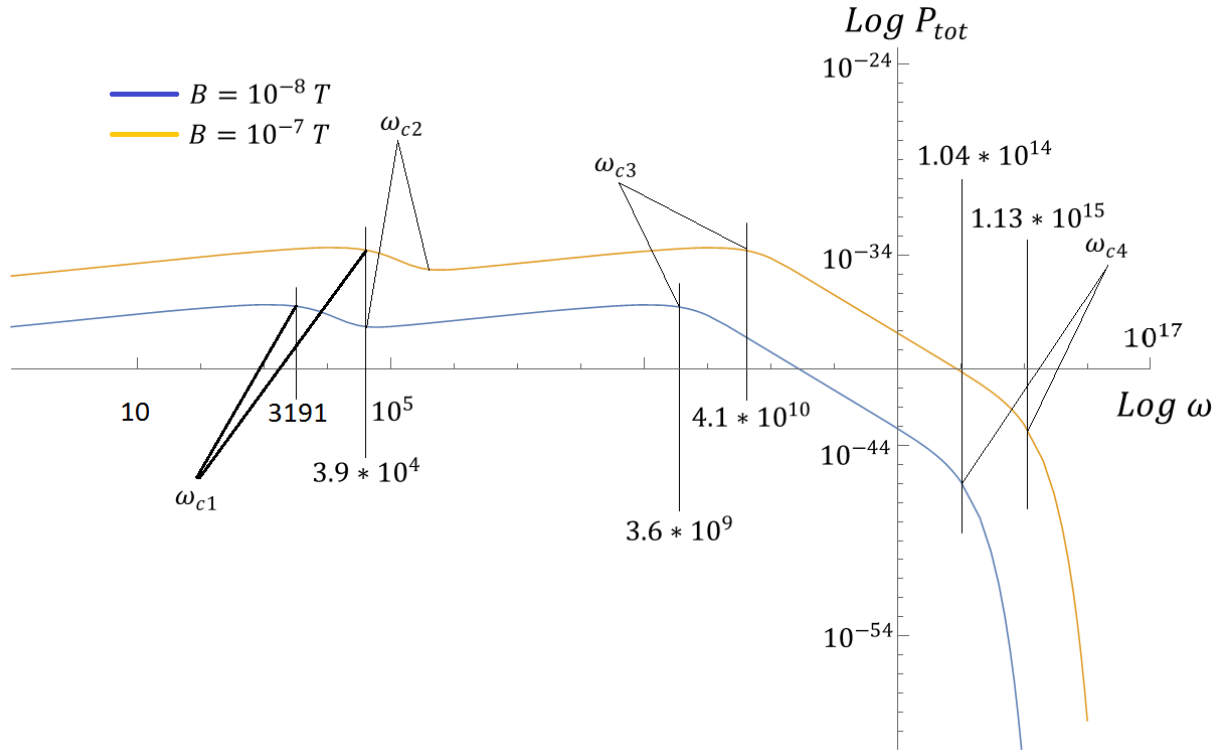
Figure 6.3: Comparison of break-frequencies when only B is changed. $\zeta = 0.999$, $k = 0.999$, $\gamma_{max} = 10^3$.
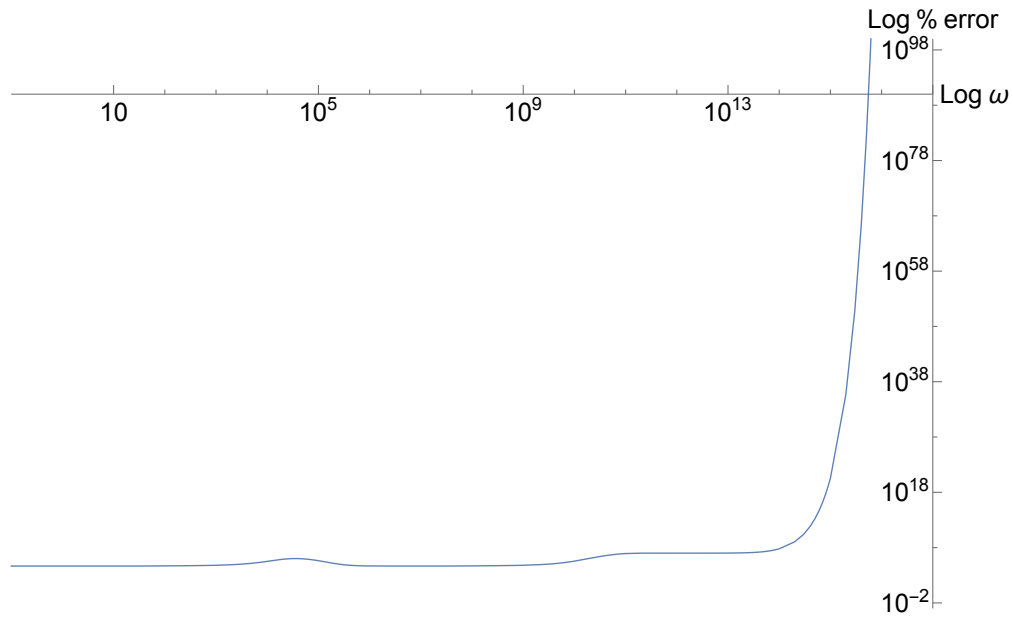
Figure 6.4: % error between composite spectra for $B = 10^{-8}$ T and $B = 10^{-7}$ T.

37

Gamma Max γ_{max}

We present a Log-Log plot of synchrotron power vs. frequency ω for three different values of γ_{max}, $\gamma_{max} = 10^2$, $\gamma_{max} = 10^3$ and $\gamma_{max} = 10^4$. The usual quadratic trend for the break-frequencies is followed here as well. The exponential cut-off frequency is the same since upper limit of γ is the same. For all cases, $B = 10^{-8}$ T and $k = \zeta = 0.999$. The second plot shows percentage error as a function of frequency for $\gamma_{max} = 10^3$ and $\gamma_{max} = 10^4$. One can see that the error initially increases with frequency and finally attains a constant value. The plot shows that γ_{max} is also a very sensitive parameter.
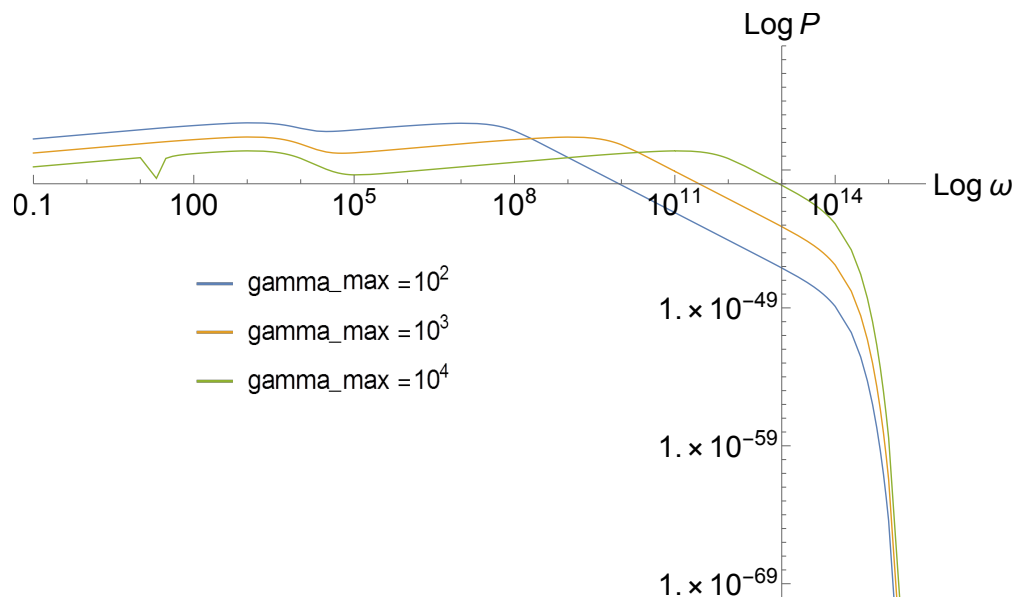
Figure 6.5: Multiple graphs for the composite spectrum with different values of γ_{max}. $B = 10^{-8}$ T and $k = \zeta = 0.999$.
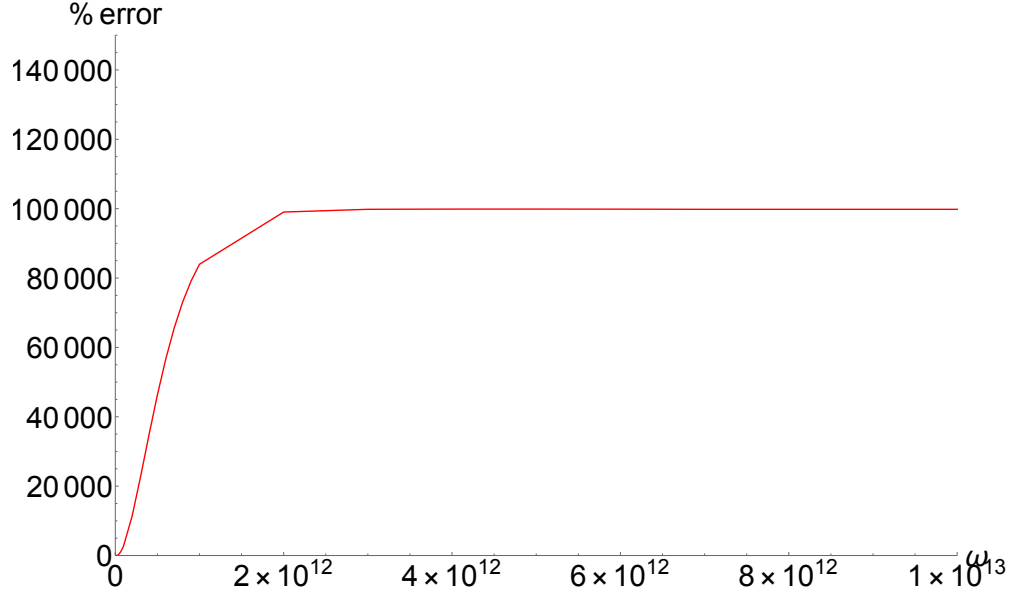
Figure 6.6: % error from a (-)900 % increase in γ value from $\gamma_{max} = 10^3$ to $\gamma_{max} = 10^4$.

Electron Number Density Ratio k

We present a Log-Log plot of total synchrotron power vs. frequency ω for four different values of the parameter $k = n_{out}/n_{in}$. It can be seen that the break-frequencies ω_{c1}, ω_{c3} and ω_{c4} do not depend on the parameter k. The values of B, γ_{max} and ζ have been taken to be 10^{-8} T, 10^3 and 0.999 respectively. The second plot is again a Log-Log plot of percentage error vs. frequency. It that the parameter k is less sensitive at higher frequencies than at lower ones.
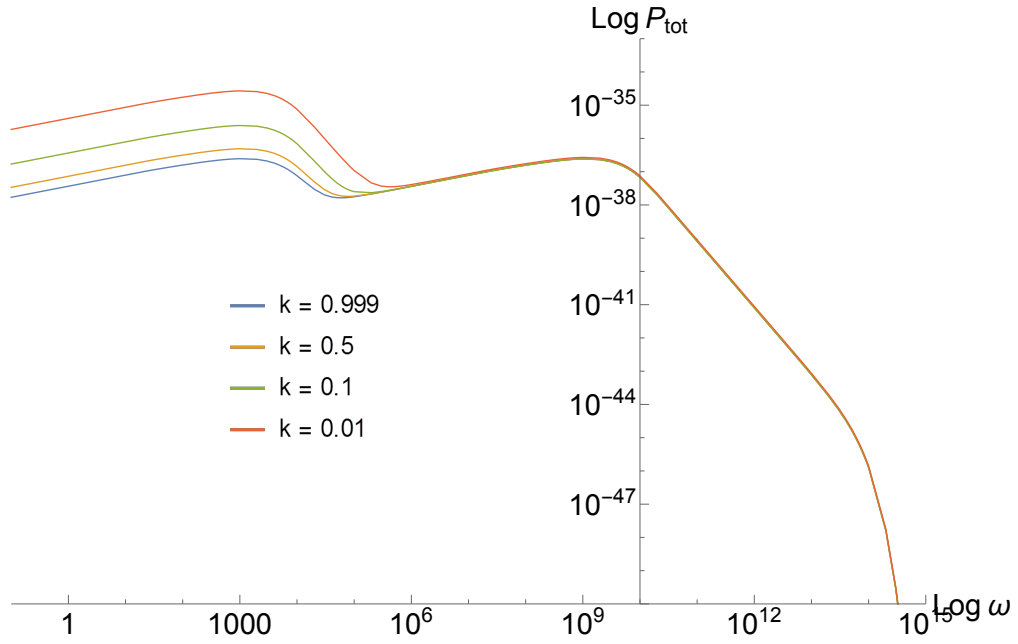
Figure 6.7: Log-Log plot of P_{tot} vs. ω. Here, $B = 10^{-8}$ T, $\gamma_{max} = 10^3$ and $\zeta = 0.999$.
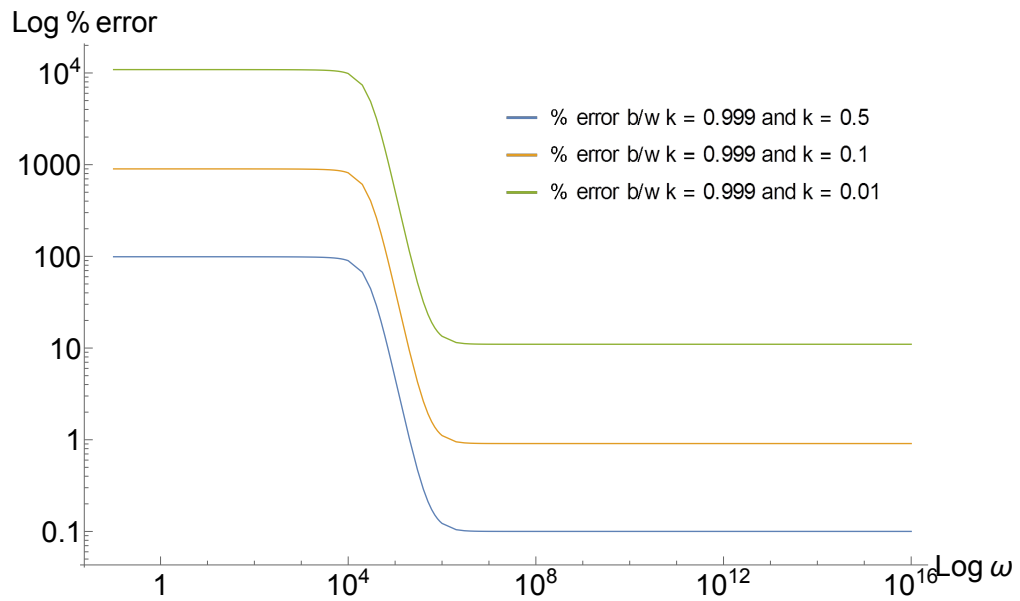
Figure 6.8: % error plot for k. One notes that it is less sensitive at higher frequencies than at lower ones.

Magnetic Field Contrast Ratio ζ

We present a Log-Log plot of total synchrotron power vs. frequency ω for four different values of the parameter $\zeta = B_{out}/B_{in}$. The plot establishes that break frequencies of the composite spectrum for the single filament case have a linear dependence on ζ. Here we have taken $k = 0.999$, $B = 10^{-8}$ T and $\gamma_{max} = 10^3$ as the reference values. The second plot is a Log-Log plot of percentage error vs. frequency for ζ. We note that it is more sensitive at lower frequencies.
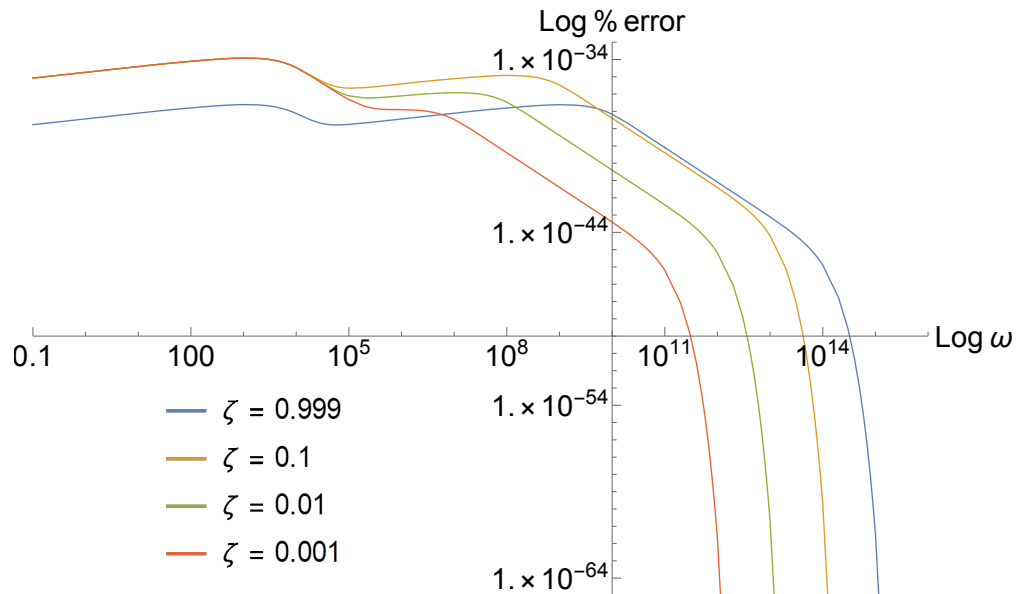
Figure 6.9: Log-Log plot of P_{tot} vs. ω with emphasis on parameter ζ. All other parameters are, $B = 10^{-8}$ T, $\gamma_{max} = 10^3$ and $k = 0.999$.
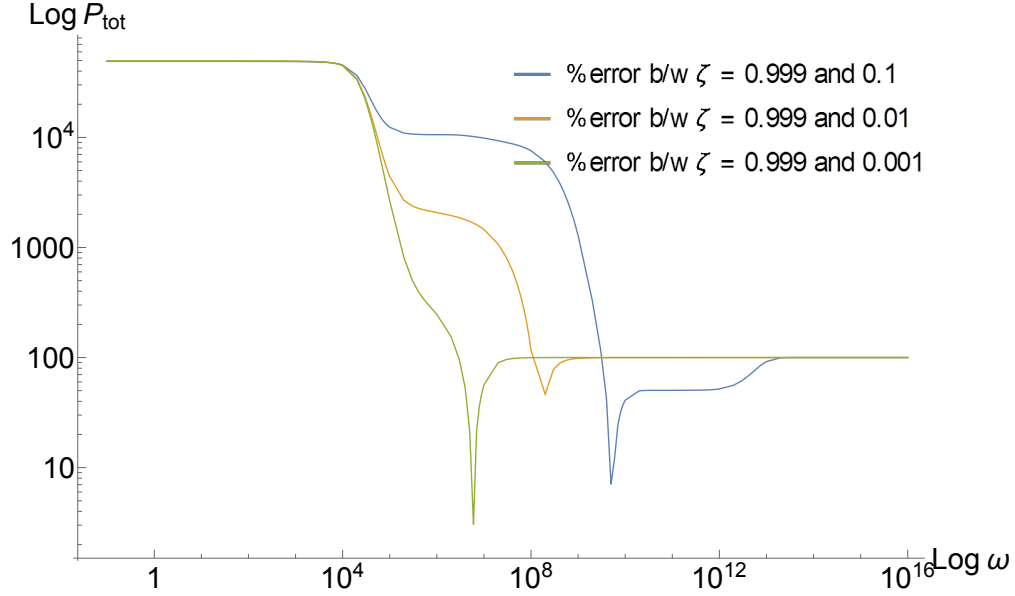
Figure 6.10: % error plot for ζ. One notes that it is more sensitive at lower frequencies.

We repeated the same procedure while keeping the % errors to a maximum of 10% and compiled the results in the following table that neatly summarizes all of them. We were thus able to conclude which parameters are the most sensitive; B_{in} and ζ are so in this case. Moreover, we came to know whether a particular independent parameter is more sensitive at higher or lower frequencies.

Parameter	% increase	% error at high ω	% error at low ω	More Sensitive At
B_{in}	$(-10, 10)$	$\sim 100, >> 100$	< 100	HIGH ω
γ_{max}	$(-10, 10)$	$\sim (30, -30)$	$\sim (-10, 10)$	HIGH ω
k	$(-5, -10)$	$\sim (0, 0)$	$\sim (-5, -11)$	LOW ω
ζ	$(-5, -10)$	$\sim (-4000, -7000)$	$\sim (-5000, -9500)$	LOW ω

Table 6.1: Parameter sensitivity as a function of frequency.

6.3 Behaviour of Break Frequencies with various Parameters

We did a thorough analysis and saw how the break frequencies depend upon the 4 independent parameters B_{in}, k, ζ and γ_{max}. We noted that there are four breaks in the composite

spectrum as opposed to just two in a uniform field case. We denote them in increasing order of frequency by ω_{c1}, ω_{c2}, ω_{c3} and ω_{c4}. These break frequencies correspond to the following values of γ: $\gamma = 1$ for ω_{c1}, $\gamma = 10^3$ for ω_{c3} and $\gamma = 10^5$ for ω_{c4}. The break at ω_{c2} is a new occurrence and cannot be predicted theoretically. The reference values of the parameters have been taken as follows: $B_{in} = 10^8$ T, $\gamma_{max} = 10^3$, $k = 0.999$ and $\zeta = 0.999$.

6.3.1 Dependence on B_{in}

We changed the reference value of the magnetic field by $\pm 50\%$ and plotted all four break frequencies as a function of the magnetic field. We then noted how the break frequencies changed and plotted the same in Mathematica. A lot of the numbers had to be guessed through naked eye which might have reduced the accuracy. However, the first break frequency seems to increase linearly with B_{in}, in accordance with $\omega_c \propto \gamma^2 B$.

(a) ω_{c1} vs. B_{in}

(b) ω_{c2} vs. B_{in}

(c) ω_{c3} vs. B_{in}

(d) ω_{c4} vs. B_{in}
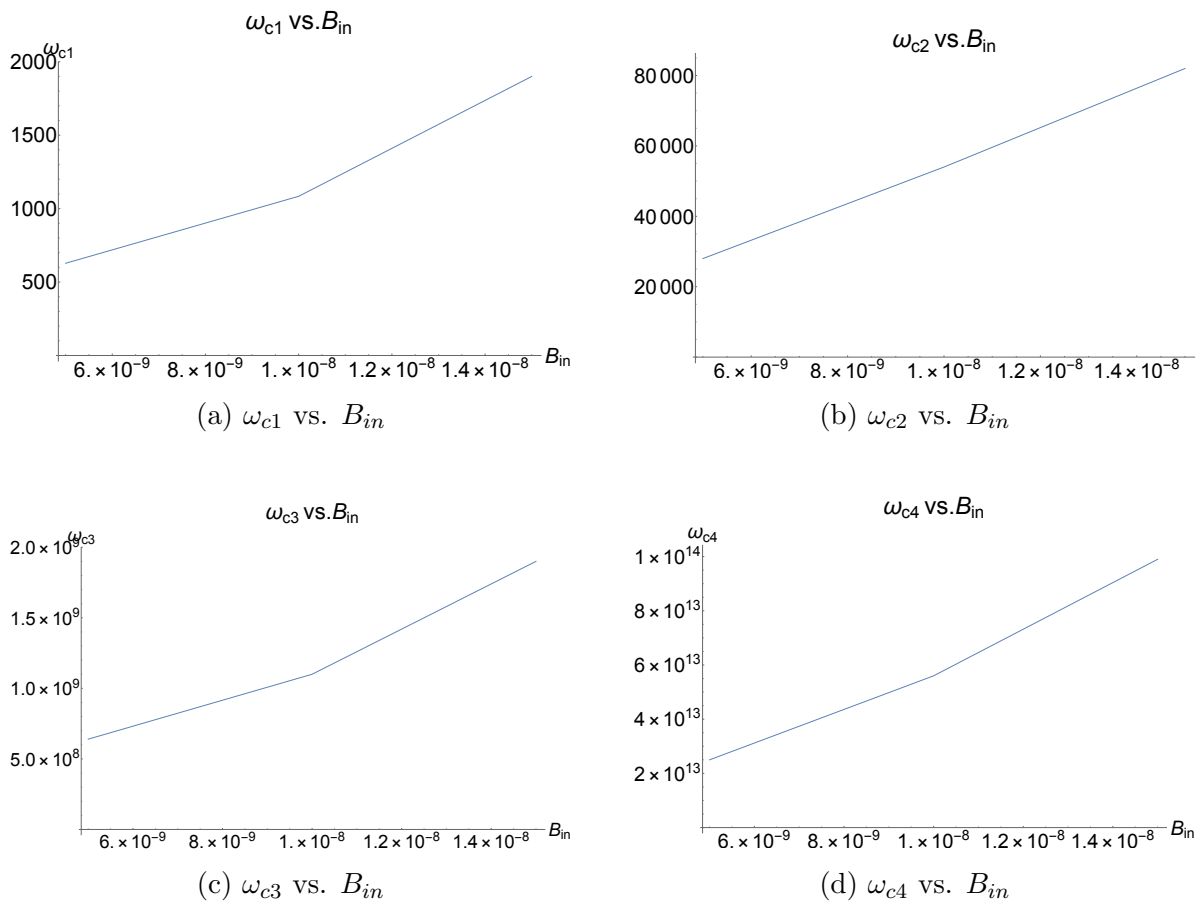
Figure 6.11: Break frequencies as a function of the Magnetic Field.

6.3.2 Dependence on γ_{max}

We changed the reference value of γ_{max} by $\pm 50\%$ and plotted all four break frequencies as its function. We then noted how the break frequencies changed and plotted the same in Mathematica. ω_{c1} and ω_{c4} should technically not depend on γ_{max} as they correspond to fixed values of γ ($\gamma = 1$ and $\gamma = 10^5$).

(a) ω_{c1} vs. γ_{max}

(b) ω_{c2} vs. γ_{max}

(c) ω_{c3} vs. γ_{max}

(d) ω_4 vs. γ_{max}
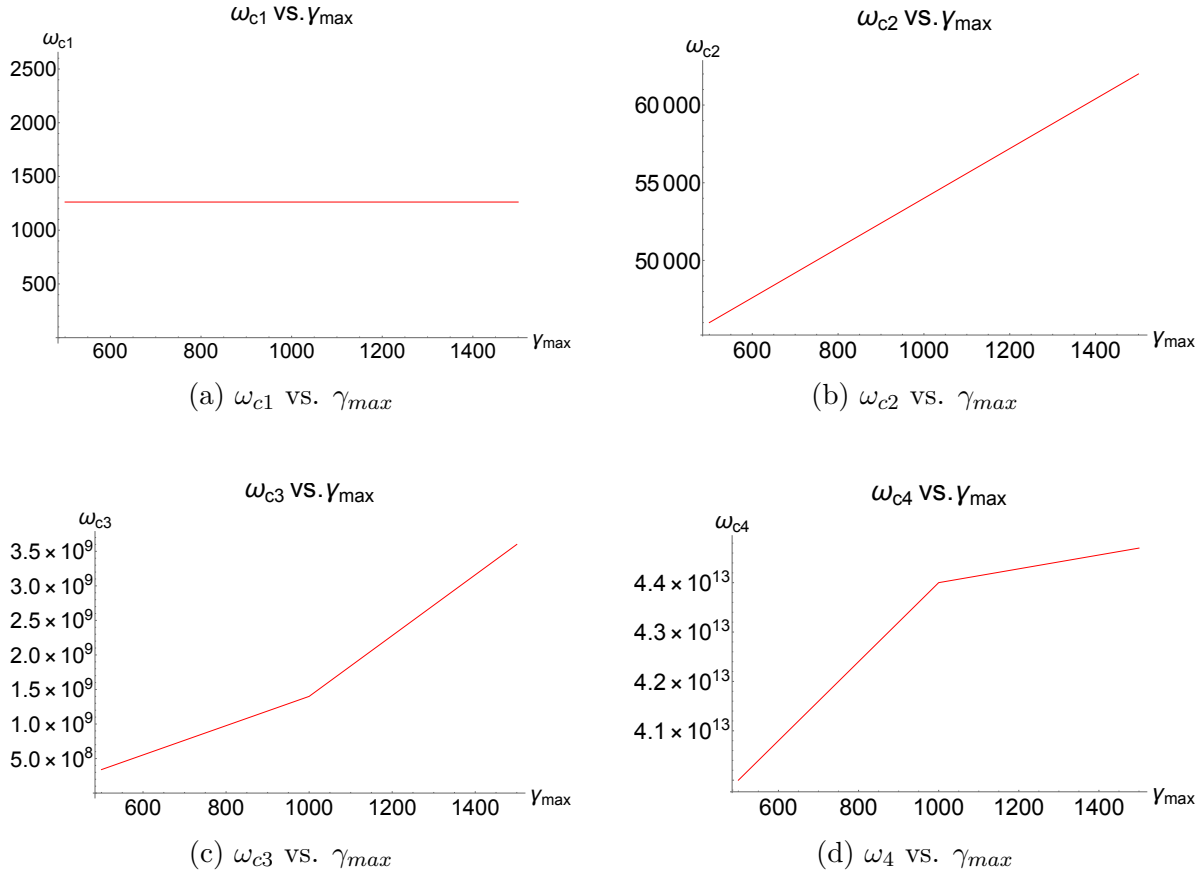
Figure 6.12: Break frequencies as a function of γ_{max}.

6.3.3 Dependence on k

The parameter k i.e. the ratio of the number density of synchrotron electrons outside and inside the filament, as is seen in the plots, influences only the second break frequencies ω_{c2}.

(a) ω_{c1} vs. k

(b) ω_{c2} vs. k

(c) ω_{c3} vs. k

(d) ω_{c4} vs. k
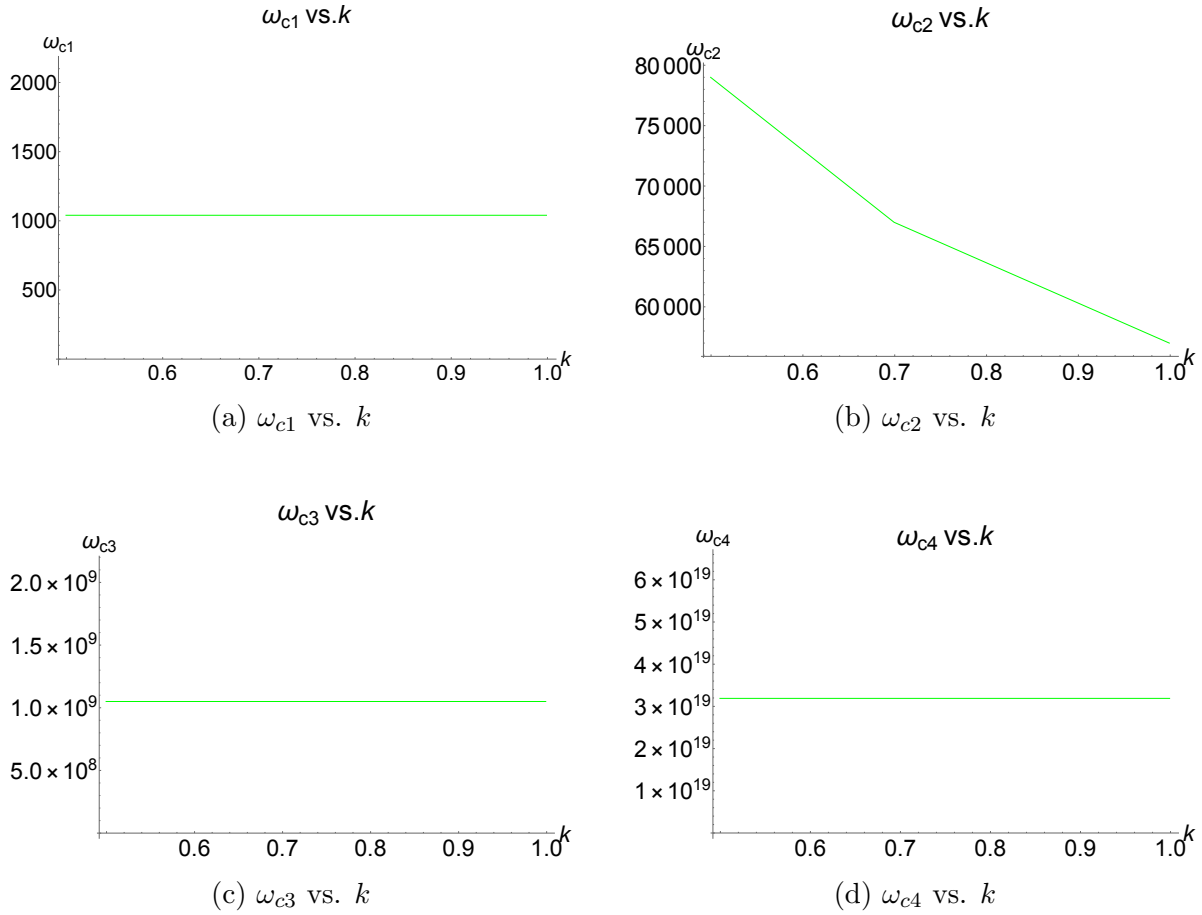
Figure 6.13: Break frequencies as a function of parameter k.

6.3.4 Dependence on ζ

The ratio of the magnetic fields from outside and inside the filament also effects the break frequencies. Although more sensitive at lower frequencies, its significance becomes greater at higher frequencies where the contribution from the background region is greater and dominant.
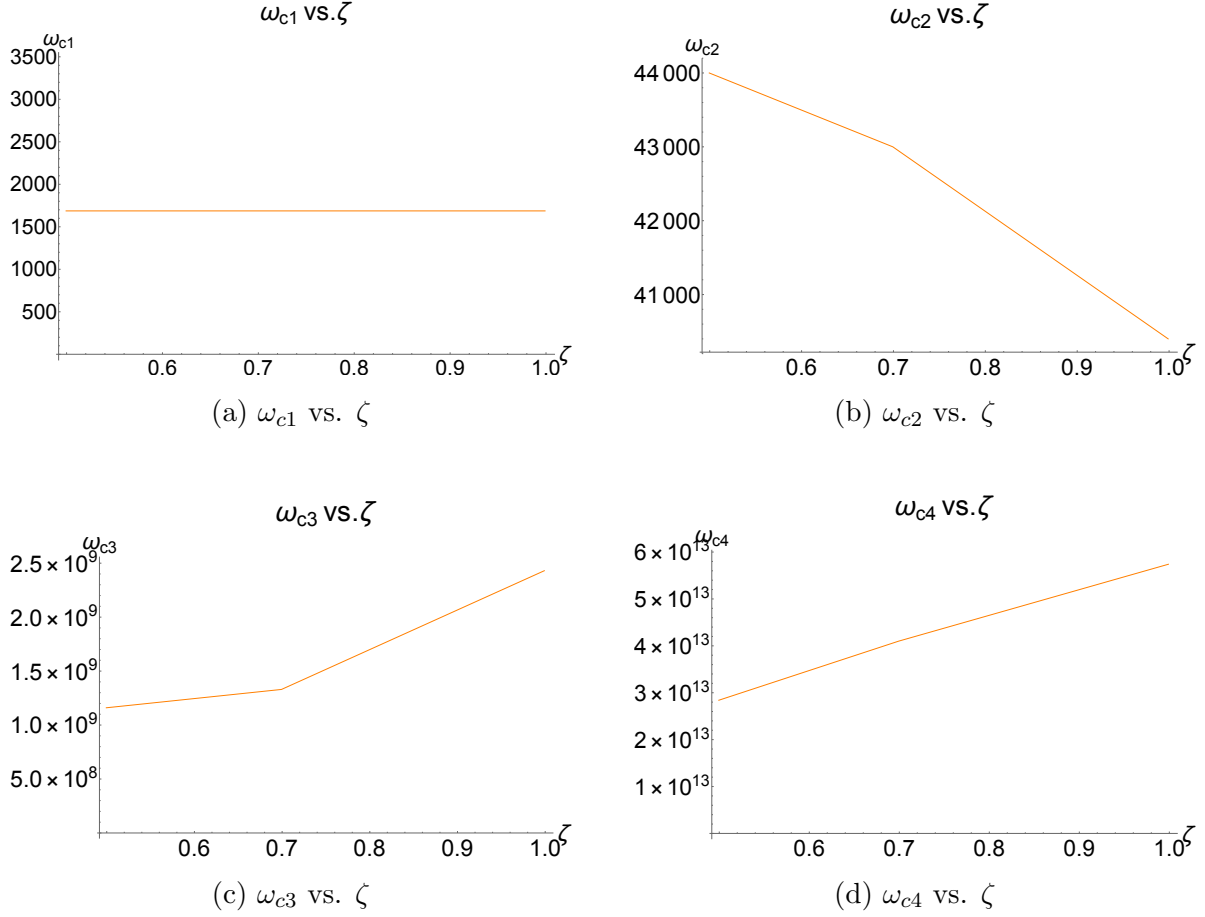
Figure 6.14: Break frequencies as a function of parameter ζ.

6.3.5 Trends of Break Frequencies

- ω_{c1} which corresponds to $\gamma = 1$ increases with B_{in} but is independent of the other three parameters γ_{max}, k and ζ.

- ω_{c2} cannot be predicted theoretically and is a new feature that arises only in the case of a composite spectrum. It increases with B_{in} and γ_{max} but decreases with k and ζ.

- ω_{c3} corresponds to $\gamma = \gamma_{max}$ and increases with B_{in}, γ_{max} and ζ. It does not seem to vary with k.

- ω_{c4} is the exponential cut-off break-frequency which occurs as a result of having a numerical upper limit on γ. In theory, the upper limit is ∞ and one observes only the power law for high frequencies all the way upto $\omega = \infty$. It shouldn't technically

depend on γ_{max} although the graph shows it to increase with the same. It increases with B_{in} and ζ but does not vary with k.

Chapter 7

Synchrotron Aging: Could the Radio Sources be Fooling Us?

7.1 Basic Theory

With regard to synchrotron radiation, the highest energy electrons are the ones to get depleted the most quickly, leading to a steepening in the emission spectrum at high frequencies over time. A synchrotron-aged radio spectrum is characterized by an (assumed) low frequency power-law emission spectrum of index p, a 'break frequency' ω_B, near which the spectrum steepens from the injected power-law, and the behavior above the break, which depends on micro-physical processes such as pitch angle scattering and particle acceleration. Assuming that the synchrotron power is the only source by which the electron loses energy, we have for highly relativistic electrons,

$$-\frac{dE}{dt} \propto B^2 E^2 \tag{7.1}$$

This clearly suggests that the higher energy electrons will radiate away their energy first. One can also calculate the characteristic timescale for a synchrotron electron with energy E (and commensurate Lorentz factor γ) by simply taking the ratio of total energy to instantaneous power,

$$\tau = \frac{E}{dE/dt} = \frac{E}{\frac{4}{3}\sigma_T c \beta^2 \gamma^2 U_B} \tag{7.2}$$

So no matter what the energy of the synchrotron electrons is, if we were to return to the blob

of plasma some time τ after it was accelerated, we would find only those electrons remaining whose lifetimes would have been longer than τ.

Mathematically, the standard radiative 'age' of the relativistic particle distribution, t_{syn}, defined as the time since the spectrum was a power-law out to infinite frequency (Eilek, Melrose & Walker, 1996), relates to ν_B and the magnetic field B through:

$$\nu_B = \frac{243 m_e^5 c^9}{64\pi e^7} B^{-3} t_{syn}^{-2}$$

For B in μG and ν_B in GHz, this can be reduced to the following convenient expression:

$$t_{syn} = 1610\, B^{-3/2}\, \nu_B^{-1/2}\, \text{MYr} \tag{7.3}$$

Relation (7.3) shows that there is an inverse relation between t_{syn} and the break frequency ν_B. This means that the break frequency decreases with time. The following diagram helps visualize the same.
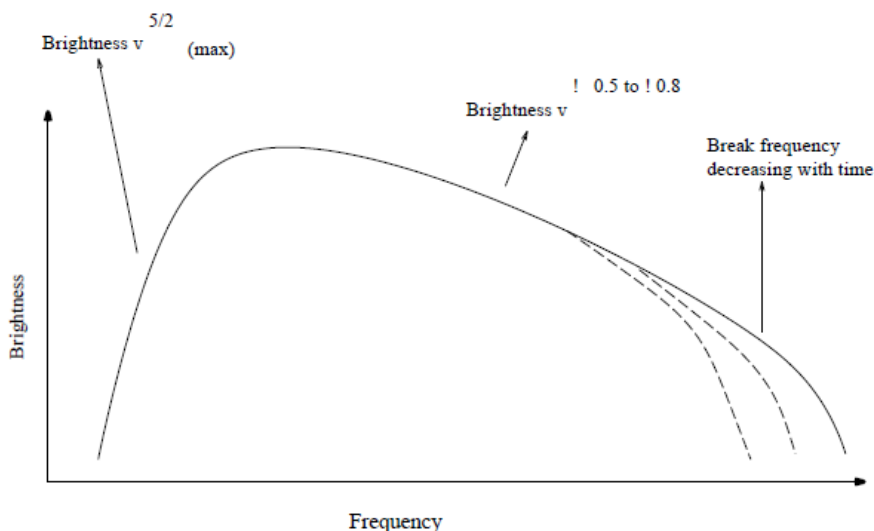

Figure 7.1: Brightness Vs. Frequency sketch showing decreasing Break Frequency with time.

7.2 The Multi-Filament Region Case

We have seen that introduction of a single filament causes the synchrotron spectra to change in a subtle but significant way. We now wish to show that a multi-filament case *can further*

complicate the phenomenon of spectral aging by introducing additional break-frequencies into the composite power spectrum. It suffices to take a 2 filament-region case for the purposes of illustration, although the same mathematical treatment can be extended to as many filaments as required.

We visualize a region of plasma with two concentric cylindrical regions having different pressures and electron number densities and use the pressure balance equations to relate multiple parameters just like we did for the single filament case.
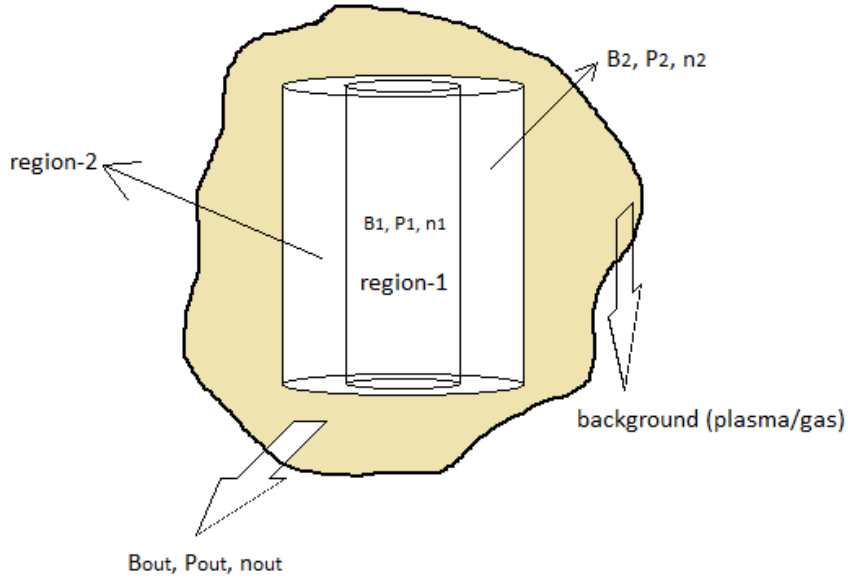
Figure 7.2: 2 Filament Region Case, two concentric cylinders are immersed in a 'weak' background.

7.2.1 Pressure Balance between Regions - 1 & 2

Assuming a state of equilibrium between region-1 and region-2, and making use of the pressure balance equation gives us the contrast ratio of the (constant) magnetic fields of these two regions. In particular, we start from,

$$\frac{B_1^2}{2\mu_o} + \int_1^{\gamma_{m1}} \gamma mc^2 K_1 \gamma^{-p} \mathrm{d}\gamma = \frac{B_2^2}{2\mu_o} + \int_{\gamma_{m1}}^{\gamma_{m2}} \gamma mc^2 K_2 \gamma^{-p} \mathrm{d}\gamma \qquad (7.4)$$

Integrating and making use of the fact that $p > 5$, we obtain the first desired relation,

$$\zeta_{21} = \left(1 - \frac{2n_1\mu_0 mc^2}{B_1^2}\left(\frac{1-p}{2-p}\right)[\gamma_{m1}k_{21} - n_1]\right)^{1/2} \tag{7.5}$$

Here $\zeta_{21} = B_2/B_1$, $k_{21} = n_2/n_1$ and γ_{m1} is the maximum possible value of the Lorentz factor for region-1. B, p and n refer to the magnetic field, the power law distribution index and the electron number density respectively. Taking ζ_{21}, k_{21}, γ_{m1} and B_1 as the independent parameters, one can solve for n_1. We shall use it in the subsequent part of the derivation.

7.2.2   Pressure Balance between Inside and Outside Regions

This time, we equate the pressures of the two inside regions to that of the outside (background) region, assuming everything to be in perfect equilibrium. In other words, we assume $P_1 = P_{out}$ and $P_2 = P_{out}$ giving respectively,

$$\frac{B_1^2}{2\mu_o} + \int_1^{\gamma_{max1}} \gamma mc^2 K_1\gamma^{-p}\mathsf{d}\gamma = \frac{B_{out}^2}{2\mu_o} + \int_{\gamma_{max1}}^{\infty} \gamma mc^2 K_{out}\gamma^{-p}\mathsf{d}\gamma \tag{7.6}$$

$$\frac{B_2^2}{2\mu_o} + \int_{\gamma_{max1}}^{\gamma_{max2}} \gamma mc^2 K_2\gamma^{-p}\mathsf{d}\gamma = \frac{B_{out}^2}{2\mu_o} + \int_{\gamma_{max1}}^{\infty} \gamma mc^2 K_{out}\gamma^{-p}\mathsf{d}\gamma \tag{7.7}$$

These can be simplified to an expression relating the contrast ratio of outside and innermost region's magnetic fields ζ_{21} with other parameters like B_1, n_1 and γ_{m2} etc. Here, $k_{out1} = k_{out}/k_1$ while γ_{m2} is the maximum possible value of the Lorentz factor for region-2. Thus equations (7.6) and (7.7) respectively reduce to:

$$\zeta_{out1} = \left(\zeta_{21}^2 + \frac{2n_1\mu_0 mc^2}{B_1^2}\left(\frac{1-p}{2-p}\right)[\gamma_{m1}k_{21} - \gamma_{m2}k_{out1}]\right)^{1/2} \quad \text{and} \tag{7.8}$$

$$\zeta_{out1} = \left(1 + \frac{2n_1\mu_0 mc^2}{B_1^2}\left(\frac{1-p}{2-p}\right)[1 - \gamma_{m1}k_{21}]\right)^{1/2} \tag{7.9}$$

We thus obtain a set of redundant but fortunately consistent equations. Equating the above two expressions makes us arrive at equation (7.5).

7.2.3 Independent Parameters

In addition to the 4 independent parameters from the single filament case, we have two more additional parameters in the 2 filament-region case. Looking at (7.5) and (7.7) there are a total of six independent parameters: ζ_{21}, k_{21}, γ_{m1}, B_1, ζ_{out1} and γ_{m2}. As mentioned earlier, we can find the number density n_1 and now in addition, k_{out1}, or equivalently, n_{out}.

7.2.4 Region-1

The total power per unit frequency as a function of frequency emitted only from region-1 can be evaluated as follows:

$$P_{tot,r1} = \frac{-n_1(-p+1)\sqrt{3}e^3 B_1}{8\pi^2\epsilon_0 cm} \int\limits_{1}^{\gamma_{m1}} F_{r1}(\omega,\gamma,B_1)\gamma^{-p}\mathrm{d}\gamma \tag{7.10}$$

Note that the approximate function $F_{apprx}(x)$ inside the integral will be different for different regions.

7.2.5 Region-2

Along similar lines, we can evaluate the total power emitted from region-2 in the following way:

$$P_{tot,r2} = \frac{-n_1 k_{21}(-p+1)\sqrt{3}e^3 \zeta_{21} B_1}{8\pi^2\epsilon_0 cm\gamma_{m1}^{-p+1}} \int\limits_{\gamma_{m1}}^{\gamma_{m2}} F_{r2}(\omega,\gamma,\zeta_{21} B_1)\gamma^{-p}\mathrm{d}\gamma \tag{7.11}$$

7.2.6 Outside (Background) Region

Finally we are left with the background region. We need to use the correct $F_{apprx}(x)$ and integrate from γ_{m2} to (technically) ∞.

$$P_{tot,bkg} = \frac{\sqrt{3}e^3 B_{out}\sin\alpha}{8\pi^2\epsilon_0 cm} \int\limits_{\gamma_{m2}}^{\infty} K_{out}F_{out}(\omega,\gamma,B_{out})\gamma^{-p}\mathrm{d}\gamma$$

$$P_{tot,bkg} = \frac{-n_1 k_{out1}(-p+1)\sqrt{3}e^3 \zeta_{out1} B_1}{8\pi^2\epsilon_0 cm\gamma_{m2}^{-p+1}} \int\limits_{\gamma_{m2}}^{\infty} F_{out}(\omega,\gamma,\zeta_{out1} B_1)\gamma^{-p}\mathrm{d}\gamma \tag{7.12}$$

7.2.7 Sum of Synchrotron Power from the 3 Regions

All that needs to be done now is to add the radiated powers from all the three regions individually. Mathematically, we need to find $P_{tot} = P_{tot,r1} + P_{tot,r2} + P_{tot,bkg}$. One can take many of the factors common so that the resulting expression for total power becomes,

$$P_{tot} = \frac{-n_1(-p+1)\sqrt{3}e^3 B_1 sin\alpha}{8\pi^2\epsilon_0 cm} \left\{ \int_{\gamma=1}^{\gamma=\gamma_{m1}} F_{r1}(\omega,\gamma,B_1)\gamma^{-p}d\gamma \right.$$

$$\left. + \frac{k_{21}\zeta_{21}}{\gamma_{m1}^{-p+1}} \int_{\gamma=\gamma_{m1}}^{\gamma=\gamma_{m2}} F_{r2}(\omega,\gamma,\zeta_{21}B_1)\gamma^{-p}d\gamma + \frac{k_{out1}\zeta_{out1}}{\gamma_{m2}^{-p+1}} \int_{\gamma=\gamma_{m2}}^{\gamma=\infty} F_{out}(\omega,\gamma,\zeta_{out1}B_1)\gamma^{-p}d\gamma \right\} \quad (7.13)$$

7.2.8 Running the Code in Mathematica

With equation (7.13) in hand, we plotted several graphs for different sets of parameters. We chose the value of p, the particle distribution index to be 5. It has been already established that p *doesn't* change the break frequencies in any way; it just changes the magnitude of values obtained for the total power. We now present the composite spectra below and also compare it with the single filament case in the limit when $B_1 = B_2$ and $n_1 = n_2$.
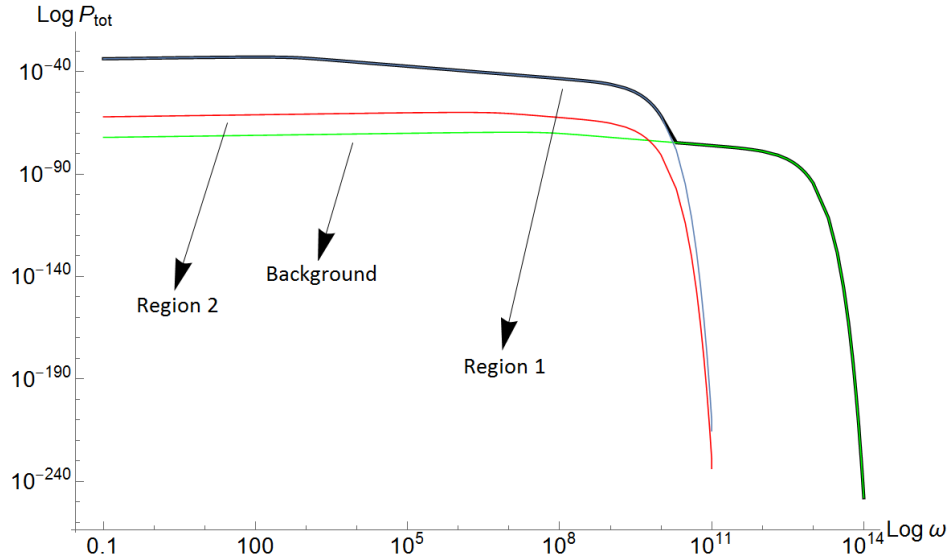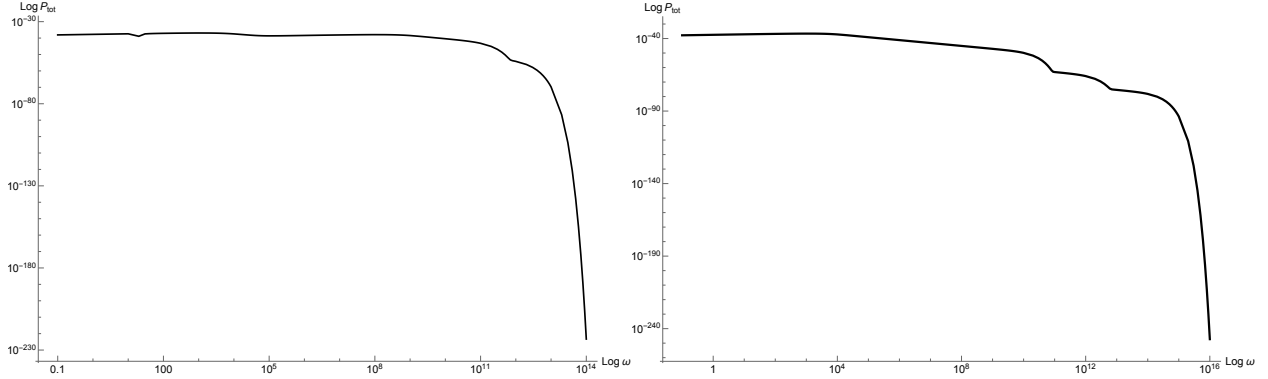

Figure 7.3: The Composite Spectra (Black). Contributions from individual regions are also visible (In Color).

(a) Synchrotron power spectrum for the single filament case.

(b) Spectrum for the 2 filament case when $B_1 = B_2$ and $n_1 = n_2$.

Figure 7.4: Comparison of single filament case with that of double filament one. Values of all the parameters are chosen to be the same for both.

7.3 Source Age from Composite Spectrum: An Artificial Example

Equation (7.3) gives the age of the synchrotron source in terms of the break frequency ν_B. Observationally, there is a possibility of mistaking the actual break frequency with the one that occurs at slightly lower frequencies as can be seen from the spectrum. This can make the source appear much older than it actually is. We shall determine the two 'ages' of the source by using the above spectrum as an example.
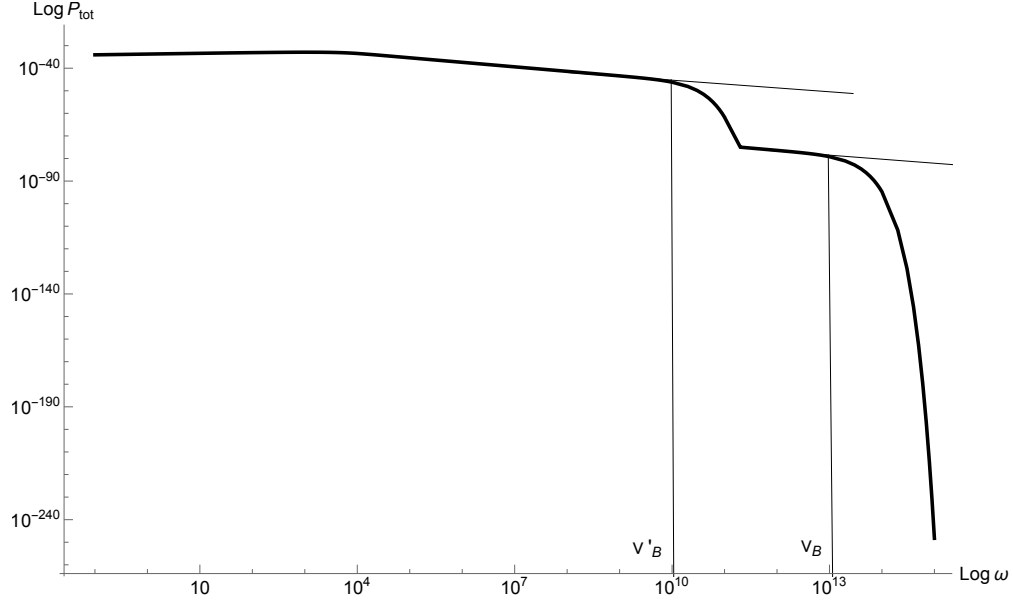
Figure 7.5: Determining the Age of the Source from Break Frequencies

We have denoted the actual break frequency by ν_B and the one that it can be mistaken with by ν'_B. The corresponding synchrotron ages are denoted by t_{syn} and t'_{syn}. Since the outside magnetic fields are much smaller than that in region-1, let us use $B = 10^{-8}\,\mathrm{T} = 100\,\mu G$. Taking $\nu_B \approx 10^4\,\mathrm{GHz}$ and $\nu'_B \approx 10\,\mathrm{GHz}$, we get,

$$t_{syn} \approx 1610 \times (10^2)^{-3/2} \times (10^4)^{-1/2} = 16100\,\mathrm{Yr} = 0.016\,\mathrm{MYr} \tag{7.14a}$$

$$t'_{syn} \approx 1610 \times (10^2)^{-3/2} \times (10)^{-1/2} = 509 \times 10^{-3}\,\mathrm{MYr} = 0.509\,\mathrm{MYr} \tag{7.14b}$$

We thus have,

$$\frac{t'_{syn}}{t_{syn}} = \frac{0.509}{0.016} = 31.81 \tag{7.15}$$

We notice that the source can look much older than it actually is. In fact in this case, it looks approximately 32 times older!

Chapter 8

Conclusion

We have been able to reproduce a part of Eilek and Arendt's paper using F_{apprx} and shown that the shape of the synchrotron spectrum varies from the standard case of a power law. We have re-confirmed that the Log-Log plot of a synchrotron spectrum for a uniform magnetic field case:

- is increasing with slope $1/3$ at lower frequencies for $\omega < \omega_{c1}$ where ω_{c1} corresponds to the lower limit of γ in the synchrotron power expression.

- is a (decaying) power law for intermediate frequencies between $\omega = \omega_{c1}$ and $\omega = \omega_{c2}$. Here ω_{c2} corresponds to the upper limit of γ.

- cuts off exponentially after $\omega = \omega_{c2}$ roughly at high frequencies.

We started with the simple case of a single filament immersed in a weaker region. The quantification of the spectrum required the use of 4 independent parameters B_{in}, contrast ratio of the magnetic fields ζ, ratio of the number densities k and the maximum possible Lorentz factor γ_{max} in contrast with only 2 parameters (B and γ_{max}) in the uniform field case.

We were able to show that the spectrum changes in a subtle but significant way and the resulting spectrum has 4 break frequencies, one of which cannot be associated with any of the γs.

We also noted that most of the contribution to the power at lower frequencies comes from the inner filament having stronger magnetic field, and that at higher frequencies comes from

outside the filament which has a weaker magnetic field. In addition, we analyzed each parameter separately and were able to pin-point whether it is more sensitive at higher or lower frequencies.

We also did the two filament region case where the role of filaments became even more clear. We showed that there can actually be another exponential cut-off frequency which might lead to wrong determination of the age of the source.

Thus, at this point, it seems quite intuitive that the number of filaments can play a major role in how the composite spectrum looks. It might add break frequencies that are otherwise absent and complicate the phenomenon of synchrotron aging.

Bibliography

[1] Eilek, J.A. and Arendt, P.N., 1994, *The Synchrotron Spectrum of Diffuse Radio Sources: Effects of Particle and Field Distributions*, The Astrophysical Journal, 457 : 150-168, 1996.

[2] Eilek, J.A., Melrose, D.B., & Walker, M.W. 1996, *Synchrotron Aging in Filamented Magnetic Fields*, The Astrophysical Journal, 483 : 282-295, 1997.

[3] Begelman M.C., Blanford, R.D., & Rees, M.J. 1984, *Theory of Extragalactic Radio Sources*, Reviews of Modern Physics, vol. 56, no. 2, part 1, 1984.

[4] Westfold, K.C. 1959, *The Polarization of Synchrotron Radiation*, Astrophysical Journal, vol. 130, p.241, 1959.

[5] Ginzburg, V.L., & Syrovatskii, S.I. 1969, *Cosmic Magnetobremsstrahlung (Synchrotron Radiation)*, Annual Review of Astronomy and Astrophysics, vol. 3 : 297-350, 1965.

[6] Carilli, C.L., Kurk, J.D., Van Der Werf, Paul, P., & Miley, G.K., *High Resolution Millimeter and Infrared Observations of the Hot Spots of Cygnus A*, The Astrophysical Journal, 118 : 2581-2591, December 1999.

[7] Longair, Malcolm S., High Energy Astrophysics, Cambridge University Press, 3rd Edition 2011.

[8] Rybicki, G.B., & Lightman, A.P., Radiative Processes in Astrophysics, pp. 400. ISBN 0-471-82759-2. Wiley-VCH, June 1986.